GLOBAL BIOGEOCHEMICAL CYCLES, VOL. 14, NO. 4, PAGES 1247-1265, DECEMBER 2000

Interannual variability of the oceanic sink of CO_2 from 1979 through 1997

Corinne Le Quéré[1], James C. Orr, Patrick Monfray and Olivier Aumont

Laboratoire des Sciences du Climat et de l'Environnement, Unité Mixte CEA-CNRS, Gif-sur-Yvette, France

Gurvan Madec

Laboratoire d'Océanographie Dynamique et de Climatologie, Université Paris VI, Paris, France

Abstract. We have estimated the interannual variability in the oceanic sink of CO_2 with a three-dimensional global-scale model which includes ocean circulation and simple biogeochemistry. The model was forced from 1979 to 1997 by a combination of daily to weekly data from the European Centre for Medium-Range Weather Forecast and the National Centers for Environmental Prediction/National Center for Atmospheric Research reanalysis as well as European Remote Sensing satellite observations. For this period, the ocean sink of CO_2 is estimated to vary between 1.4 and 2.2 Pg C yr^{-1}, as a result of annually averaged interannual variability of ± 0.4 Pg C yr^{-1} that fluctuates about a mean of 1.8 Pg C yr^{-1}. Our interannual variability roughly agrees in amplitude with previous ocean-based estimates but is 2 to 4 times less than estimates based on atmospheric observations. About 70% of the global variance in our modeled flux of CO_2 originated in the equatorial Pacific. In that region, our modeled variability in the flux of CO_2 generally agreed with that observed to ± 0.1 Pg C yr^{-1}. The predominance of the equatorial Pacific for interannual variability is caused by three factors: (1) interannual variability associated with El Niño events occurs in phase over the entire basin, whereas elsewhere positive and negative anomalies partly cancel each other out (e.g., for events such as Antarctic Circumpolar Wave and the North Atlantic Oscillation); (2) dynamic processes dominate in the equatorial Pacific, whereas dynamic, thermodynamic, and biological processes partly cancel one another at higher latitudes; and (3) our model underestimates the variability in ocean dynamics and biology at high latitudes.

1. Introduction

Interannual variability in atmospheric CO_2 provides clues which can be exploited to help unravel the relative roles of the ocean and terrestrial biosphere in absorbing and releasing atmospheric CO_2. Although changes in atmospheric CO_2 are well documented [*Keeling et al.*, 1989; *Conway et al.*, 1994; *Tans et al.*, 1996], interannual changes in sea-air flux of CO_2 are poorly constrained. Figure 1 illustrates the present controversy. Relatively small interannual variability in the sea-air flux of CO_2 (± 0.1 to ± 0.5 Pg C yr^{-1}) is deduced from measurements of oceanic partial pressure of CO_2 (pCO_2) in the equatorial Pacific [*Feely et al.*, 1987; *Inoue and Sugimura*, 1992; *Wong et al.*, 1993; *Feely et al.*, 1997; 1999; *Boutin et al.*, 1999]. However, these measurements come from only the equatorial Pacific. It cannot be excluded that other regions also contribute significantly to interannual variability. On the other hand, *Winguth et al.* [1994] found, with a three-dimensional global ocean model, that the variability in sea-air flux was $\sim \pm 0.3$ Pg C yr^{-1} and was produced mostly by the equatorial Pacific (after annually averaging as in Figure 1). Furthermore, a recent study by *Lee et al.* [1998] also found small global variability of ± 0.2 Pg C yr^{-1} using the observed seasonal relationship between sea surface temperature (SST) and pCO_2 to extrapolate the interannual variability. In contrast, much larger interannual variability in sea-air flux of CO_2 (± 1 to ± 2 Pg C yr^{-1}) is found by studies that use inverse atmospheric models and measurements of atmospheric CO_2 and ^{13}C (Figure 1) [*Keeling et al.*, 1995; *Francey et al.*, 1995; ?; *Joos et al.*, 1999]. Estimates from the last three studies use the same atmospheric ^{13}C data with different inverse methods. They vary in amplitude more than in phase, although the estimates by *Keeling*

[1]Now at Max-Planck-Institut für Biogeochemie, Jena, Germany

Paper number 1999GB900049.
0886-6236/00/1999GB900049$12.00

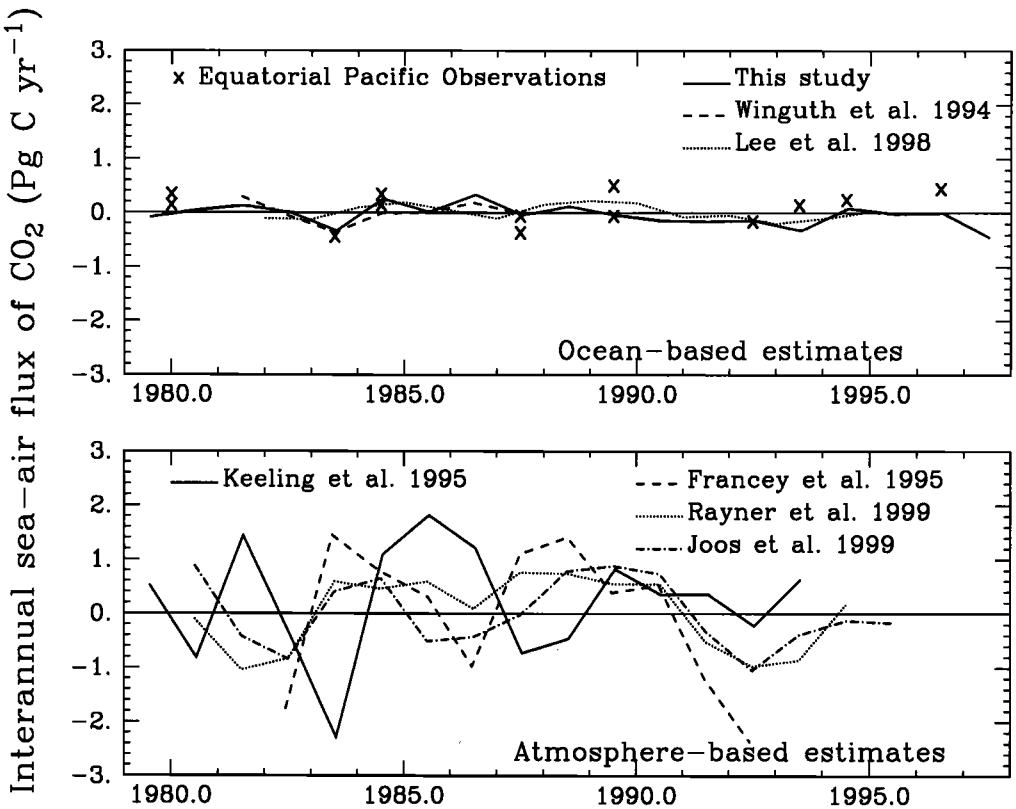

Figure 1. Time series of the interannual sea-to-air flux of CO_2 as estimated using (top) ocean observations and models and (bottom) atmospheric observations and models. All results were annually averaged. All studies represent the global oceans except the equatorial Pacific fluxes, which are based on observations. Those estimates were summarized by *Feely et al.* [1997] and include data compiled by *Keeling and Revelle* [1985], *Smethie et al.* [1985], *Takahashi et al.* [1986], *Feely et al.* [1987], *Volk* [1989], *Inoue and Sugimura* [1992], *Wong et al.* [1993], and *Feely et al.* [1995, 1997, 1999]. An average value of 0.57 was subtracted from the estimates to obtain the flux anomalies.

et al. [1995], who use ^{13}C data from a different source, are clearly out of phase with the others.

One advantage to using forward studies with an ocean model, such as that used by *Winguth et al.* [1994], is that results can be evaluated by comparison with physical and geochemical measurements. An outstanding effort has been made in recent years to summarize observations from the past 2 decades in the equatorial Pacific [*Boutin and Etcheto,* 1997; *Feely et al.*, 1997, 1999], thereby offering a benchmark to gauge model-estimated variability. Our study benefits from this effort, and we can make the extra step beyond *Winguth et al.* [1994] to confront the model results with observations in that region. Unfortunately, other oceans have fewer data as well as a relatively larger seasonal cycle when compared to interannual variability. In this paper, we emphasize the data-based evaluation of modeled sea-air fluxes, and we focus on three regions: (1) the equatorial Pacific where El Niño events cause large interannual changes in ocean dynamics and geochemistry [*Keeling and Revelle*, 1985]; (2) the Southern Ocean where the Antarctic Circumpolar Wave (ACW) perturbs the ocean dynamics [*Jacobs and Mitchell*, 1996] over 20% of the ocean surface; and (3) the North Atlantic where the North Atlantic Oscillation (NAO) is well documented [*Hurrell*, 1995].

We have investigated the interannual variability of the ocean's carbon cycle with an ocean general circulation model (OGCM) which has relatively high resolution at the equator (0.5°). Such resolution is necessary to properly resolve the key dynamical features of the equatorial region, such as the equatorial undercurrent. Other specificities of our model simulations include a prognostic model of vertical turbulence, important at the equator, where there is large current shear, and daily to weekly forcing for heat and water fluxes, wind stress, and wind speed. The good equatorial dynamics of our OGCM is an improvement compared to that of *Winguth et al.* [1994], but, except for surface alkalinity, we used the same ocean biogeochemistry model.

The following sections detail the model, describe and evaluate the interannual variability of the simulated ocean dynamics in the three chosen regions, and describe and evaluate interannual variability of surface

oceanic pCO_2 in the equatorial Pacific and of the sea-air flux of CO_2 in the global ocean. Finally, we discuss the processes that drive the variability in sea-air flux of CO_2 in the model.

2. Model Description

2.1. Dynamic Model

We used a global OGCM developed at the Laboratoire d'Océanographie Dynamique et de Climatologie (LODYC, Paris), OPA 8.0 (Océan Parallélisé) [*Madec et al.*, 1997; *Madec and Imbard*, 1996; *Guilyardi and Madec*, 1997]. For our study we used OPA in the configuration described by *Aumont et al.*, [1998, 1999].

The spatial resolution of OPA is roughly equivalent to a geographical mesh of 2° of longitude by 1.5° of latitude, with an increased latitudinal resolution of 0.5° near the equator. OPA has 30 vertical levels, with 10 levels in the top 100 m. The horizontal mesh is orthogonal and curvilinear on the sphere. The northern singularity of the grid, where meridional grid lines converge, has been shifted to be over the Asian continent [*Madec and Imbard*, 1996]. Vertical eddy diffusivity and viscosity coefficients are computed from a 1.5 order turbulent closure scheme which has an explicit formulation of the mixed layer, as well as minimum of diffusion in the thermocline [*Gaspar et al.*, 1990; *Blanke and Delecluse*, 1993]. In the vertical, the minimum background diffusion is set to 10^{-5} m^2 s^{-1} [*Ledwell et al.*, 1998]. To further improve the parameterization of vertical mixing, solar radiation is allowed to penetrate in the top few meters of the ocean instead of being imposed at the surface only [*Blanke and Delecluse*, 1993]. We run the model in a semidiagnostic mode: temperature and salinity are restored toward the climatological observations of *Levitus* [1982] in the interior of the ocean, below the mixed layer, away from ocean-land boundaries [*Aumont et al.*, 1998]. The restoring time constant is variable and has a value of 1 $year^{-1}$ in the deep ocean and 1 $month^{-1}$ just below the mixed layer. This restoring term is not applied in the equatorial region between 10°S and 10°N. This semidiagnostic method forces the ocean interior to maintain its observed averaged seasonal variations but permits interannual variability in the equatorial ocean and everywhere in the mixing layer.

The forcing and initialization procedure is summarized in Table 1. For the period from 1979 to 1993, we used daily wind stress and wind speed data from the European Centre for Medium-Range Weather Forecasts (ECMWF) reanalysis [*Gibson et al.*, 1997]. After 1993, ECMWF reanalysis is not available. Thus we used weekly wind stress and wind speed from the European Remote Sensing (ERS 1 and 2) satellite observations. However, during the latter period we normalized to ECMWFs wind stress fields by first time averaging ECMWF and ERS wind fields over the year 1993, when both data sets are available, and then adding the ECMWF-ERS difference to ERS. The normalization insures that the spatial distribution of the wind stress is consistent before and after 1993, although the time fluctuations are from different sources (Table 1). For the entire experiment from 1979 to 1997, we used daily heat and water fluxes from the National Centers for Environmental Prediction/National Center for Atmospheric Research (NCEP/NCAR) reanalysis [*Kalnay et al.*, 1996]. The ECMWF and NCEP/NCAR produced surface values of the above fields over the globe by assimilating, in their respective atmospheric models, observations of wind speed, SST, ice cover, air pressure, and humidity [*Uppala*, 1997]. Although ECMWF provides heat and water fluxes, we have chosen not to use them because the global water fluxes and latent heat fluxes showed decadal variations larger than a sverdrup, which is more than the total river runoff and not documented by observations. The water fluxes from NCEP/NCAR are conserved globally and seemed more realistic. However, the wind fields from ECMWF were kept, as they gen-

Table 1. Summary of Model Forcing and Initialization Fields

	First Equilibration	Second Equilibration	1979-1993	1994-1997
Wind stress	HR (mc)	ECMWF (d)	ECMWF (d)	ERS (w) plus ERS93'
Wind speed	SSMI (mc)	ECMWF (d)	ECMWF (d)	ERS (w) plus ERS93'
Heat fluxes	*Oberhuber* [1988] (mc)	NCEP/NCAR (d)	NCEP/NCAR (d)	NCEP/NCAR (d)
Water fluxes	*Oberhuber* [1988] (mc)	NCEP/NCAR (d)	NCEP/NCAR (d)	NCEP/NCAR (d)
SST	*Levitus* [1982] (mc)	RS (w)	RS (w)	RS (w)
SSS	*Levitus* [1982] (mc)	*Levitus* [1982] (mc)	constant correction	constant correction
TALK	HAMOCC3	—	equation 4	equation 4

The results presented in this paper are the simulations from 1979 to 1997, described in the last two columns. The first equilibration is described by Aumont et al. [1998]. Abbreviations are defined as follows: d, daily; w, weekly; mc, monthly climatology; ECMWF, European Centre for Medium-Range Weather Forecasts; NCEP/NCAR, National Centers for Environmental Prediction/National Center for Atmospheric Research; ERS, European Remote Sensing; HR, *Hellerman and Rosenstein* [1983]; RS, *Reynolds and Smith* [1994]; SSMI, the Geosat altimeter special remote sensor microwave/imager; ERS93', the local difference between ECMWF and ERS wind fields averaged over the year 1993; SST, sea surface temperature; SSS sea surface salinity; TALK, total alkalinity; HAMOCC3, Hamburg model of the oceanic carbon cycle.

erate a reasonable wind-driven circulation in the equatorial oceans.

Besides imposing a heat flux at the ocean surface, we also allow retroaction between modeled SST and weekly satellite observations of SST [*Reynolds and Smith*, 1994]. The total heat flux Q at the surface of the model ocean, with positive values when the atmosphere gains heat, is defined as

$$Q = Q_0 + \frac{dQ}{dt}(\mathrm{SST_{mod}} - \mathrm{SST_{obs}}) \quad (1)$$

where Q_0 is the heat flux as prescribed by NCEP/NCAR and dQ/dt is the model's constant based on the linearized bulk formulas (40 W m^{-2} K^{-1}). The dQ/dt term is equivalent to 48 $days^{-1}$ for a mixed layer of 40 m. In OPA though, the mixed layer varies in space and time as a function of the turbulent closure scheme. The $\mathrm{SST_{mod}}$ and $\mathrm{SST_{obs}}$ terms are the modeled and observed SSTs, respectively. We also restored ice cover toward the weekly ice cover deduced from the observed SST, with a time constant equivalent to that of the heat retroaction [*Aumont et al.*, 1998].

Unfortunately, no global salinity observations are available for the interannual timescale. To maintain a reasonable interannual water flux signal while avoiding large drift in the surface salinity, we applied a correction to the surface salinity which was spatially variable but constant in time (J. Vialard, personal communication 1998). This correction W_{CORR} was computed by running the model a first time from 1979 to 1993 while restoring surface salinities to climatological values (Table 1). Then the restoring term for salinity from this run was averaged temporally from 1979 to 1993, and smoothed horizontally using an influence radius of 555 km [*Levitus*, 1982]. The resulting field is used as a correction to the free model. The total water flux W at the surface of the model ocean is therefore

$$W = W_0 + W_{\mathrm{CORR}} \quad (2)$$

where W_0 is the water flux as prescribed by NCEP/NCAR. All the terms of (2) vary spatially, but only W_0 and thus W vary interannually; W_{CORR} is constant in time. Therefore the surface salinity of the ocean model does undergo interannual variability.

2.2. Ocean Biogeochemistry Model

The geochemical tracers included in this study are dissolved inorganic carbon (DIC), total alkalinity (TALK), O_2, $CaCO_3$, PO_4^{3-}, dissolved silicate, and particulate organic carbon (POC), which are all transported as passive tracers in the ocean. The concentration of DIC, of particular interest to this study, varies according to the following set of equations:

$$\frac{d\mathrm{DIC}}{dt} = J_{\mathrm{DYN}} + J_{\mathrm{WF}} - J_{\mathrm{CO_2}} - J_{\mathrm{BIO}} \quad (3a)$$

$$J_{\mathrm{DYN}} = -\mathbf{v}\cdot\nabla\mathrm{DIC} + \nabla\cdot(\kappa\nabla\mathrm{DIC}) \quad (3b)$$

$$J_{\mathrm{WF}} = (E-P)S\frac{\mathrm{DIC}^*}{S^*} \quad (3c)$$

$$J_{\mathrm{CO_2}} = \frac{F_{\mathrm{CO_2}}}{\Delta Z} \quad (3d)$$

$$F_{\mathrm{CO_2}} = k_g(1-\gamma_{\mathrm{ice}})[p\mathrm{CO_{2_{oc}}} - p\mathrm{CO_{2_{atm}}}] \quad (3e)$$

where the J terms represent all sources and sinks of DIC. J_{DYN} represents the transport by ocean dynamics, and J_{WF} is the concentration or dilution of DIC due to freshwater flux at the surface. $J_{\mathrm{CO_2}}$ represents the sea-to-air exchange of carbon, which is applicable only in the surface layer. Since $J_{\mathrm{CO_2}}$ is positive when the atmosphere gains CO_2, it has a minus sign in (3a). Finally, J_{BIO} represents the biological sources and sinks of CO_2. Since J_{BIO} is positive when carbon is exported out of the mixed layer, it also has a minus sign in (3a).

The ocean dynamics term J_{DYN} (equation (3b)) includes advection and diffusion, with $\mathbf{v}$ and κ being the velocity vector and diffusion tensor, respectively. Advection is implemented using the numerical scheme of *Smolarkiewicz and Clark* [1986], which is only slightly diffusive and ensures that the concentration of passive tracers remains positive. Tracers are advected and diffused along horizontal surfaces. The dilution term J_{WF} (equation (3c)) accounts for the effect of precipitation P and evaporation E with S being the model's local salinity, and DIC^* and S^* are the global mean concentrations of DIC and S respectively, for the preindustrial ocean surface. This correction is necessary because the volume of the ocean's surface layer is fixed in the model, as imposed by the model's rigid-lid approximation [*Sarmiento et al.*, 1995; *Murnane et al.*, 1999].

The flux of carbon $F_{\mathrm{CO_2}}$ from sea to air is related to the DIC concentration by the depth of the surface layer ΔZ (equation (3d)). Equation (3e) details $F_{\mathrm{CO_2}}$, where k_g is the wind-speed-dependent gas exchange coefficient of *Wanninkhof* [1992] corrected for chemical enhancement, γ_{ice} is the fraction of the sea surface covered by ice, and $p\mathrm{CO_{2_{oc}}}$ is the partial pressure of CO_2 at the surface of the ocean computed as a function of DIC, TALK, temperature, and salinity, using the solubility formulation of *Weiss* [1974] and dissociation constants from *Edmond and Gieskes* [1970]. The final term, $p\mathrm{CO_{2_{atm}}}$ is the partial pressure of CO_2 in the atmosphere, maintained at its preindustrial value of 278 ppm throughout the simulation.

To account for the increase of atmospheric CO_2 since the preindustrial era and to compare model results directly with observed $p\mathrm{CO_{2_{oc}}}$, we also modeled the anthropogenic CO_2 flux and its interannual variability as a separate tracer. To do so, we included a tracer representing only the fraction of CO_2 which penetrated into the ocean since the preindustrial era [*Siegenthaler and Joos*, 1992; *Sarmiento et al.*, 1992]. The flux of anthropogenic CO_2 is then calculated using an equation similar to (3e) but with $p\mathrm{CO_{2_{oc}}}$ and $p\mathrm{CO_{2_{atm}}}$ representing only the oceanic and atmospheric perturbations, respectively, in CO_2 relative to preindustrial values. Although the perturbation method assumes the carbon

cycle is in steady state, which is not exact for interannual simulations, a sensitivity study where we added the anthropogenic component to the natural cycle reproduced the same variability to ± 0.05 Pg C yr^{-1}. In this latter simulation, however, it is not possible to separate the drift from the ocean sink, thus we present the results of the former simulation. For the anthropogenic component, $pCO_{2_{atm}}$ is forced to follow a spline fit to the Mauna Loa plus ice core data [*Enting et al.*, 1994], which have no interannual variability. Neglecting the interannual variability caused by $pCO_{2_{atm}}$ leads to a maximum error of $\sim \pm 0.1$ Pg C yr^{-1}. This number represents the flux of CO_2 (equation (3e)) computed with $pCO_{2_{atm}}$ being the departure from the spline fit used in this study and $pCO_{2_{oc}}$ being the ocean response estimated using the pulse functions of *Sarmiento et al.* [1992] [*Joos et al.*, 1996]. Results presented in this paper include both the natural and anthropogenic components.

Finally, the biological sources and sinks J_{BIO} were computed using the Hamburg model of the oceanic carbon cycle (HAMOCC3) [*Maier-Reimer*, 1993] coupled to OPA [*Aumont*, 1998; *Aumont et al.*, 1999]. This biogeochemical model computes export production defined here as that part of biological production transported below the euphotic zone (top 50 m). In HAMOCC3, export production is a function of phosphate availability, temperature, mixed-layer depth, and light. Of those four controls, only light does not vary interannually in our simulation. The export production is instantaneously transferred into particulate organic carbon below the euphotic zone according to the profile of *Suess* [1980], where it is remineralized at a rate that depends on temperature [*Maier-Reimer*, 1993].

The production of hard shells is made by favoring silicate to calcite and therefore depends both on the local concentration of silicate and export production. The resulting ratio of production of carbonate shells to that of soft tissue (rain ratio) is 0.22. That is 3 times the proposed rain ratio of 0.08 by *Yamanaka and Tajika* [1996] which was adjusted in their OGCM to match observed vertical profiles of alkalinity. Our mean vertical profile of alkalinity is 2 to 3 times steeper than observed in the top 300 m of the ocean. As a means to correct the variations of TALK at the surface, we recalculate it by relying on the observed linearity between TALK and S. We parameterized interannual variability in surface TALK as a linear function of S, which varied about the modeled climatological monthly mean TALK ($\overline{\text{TALK}}$), as described below:

$$\text{TALK}(x,y,t) = \overline{\text{TALK}(x,y,m)} + \text{TALK}_{\text{GEOSECS}} \left[\frac{S(x,y,t) - \overline{S(x,y,m)}}{\overline{S(x,y,m)}} \right] \quad (4)$$

where x and y are the longitude and latitude, t is the time, and m is the month. $\text{TALK}_{\text{GEOSECS}}$ is the mean surface TALK of 2310 μeq kg^{-1} as determined from Geochemical Ocean Sections Study (GEOSECS) measurements [*Takahashi et al.*, 1981]. $\overline{\text{TALK}}$ and $\overline{S}$ are computed by running the model a first time in the standard configuration of HAMOCC3 from 1979 to 1993, with no correction for TALK and with a restoring term to surface salinity (Table 1). Our alkalinity parameterization ensures that the long-term average pCO_2 at the surface remains constant, that it is consistent with the equilibrium model run of *Aumont et al.* [1999] which was used to initialize the model, and that it varies according to the observed linearity between TALK and salinity.

For this study of interannual variability, the HAMOCC3 biogeochemical model has its limitations. First, it responds slowly to seasonal changes owing to its long time constants. The largest impact is found in the high northern latitudes, where the modeled seasonality of pCO_2 has about half the amplitude and lags 4 months behind the observations [*Six and Maier-Reimer*, 1996; *Aumont*, 1998]. Second, HAMOCC3 underestimates biological productivity in the subtropical gyres, by 40% compared to the Joint Global Ocean Flux Study (JGOFS) observations [*Karl and Lukas*, 1996; *Lohrenz et al.*, 1992]. The cause is HAMOCC3's biological limitation based on phosphate only and its absence of dissolved organic carbon [*Aumont*, 1998]. Third, HAMOCC3 overestimates the productivity in the eastern equatorial Pacific, by ~100% compared with the estimates of *Jianrong and Quay* [1997]. That is also caused by the absence of DOC, as well as the absence of grazing by zooplankton and the absence of iron limitation [*Six and Maier-Reimer*, 1996; *Aumont*, 1998; *Stoens et al.*, 1998; *Coale et al.*, 1996]. On the other hand, when HAMOCC3 is coupled to the OPA circulation model, one finds very little excess subsurface nutrients (nutrient trapping) in the equatorial Pacific [*Aumont et al.*, 1999]. Nutrient trapping is a problem common in other coarse-resolution models. The absence of nutrient trapping is due to the improved equatorial dynamics in OPA. Our working hypothesis was that the interannual variations based on nonabrupt changes in the dynamics will be reasonably well reproduced by HAMOCC3, whereas the abrupt dynamic changes occurring over a few weeks will not be captured entirely.

We initialized our biogeochemical model with the equilibrium output from the off-line carbon simulation of *Aumont et al.* [1999], which was forced by monthly mean climatological heat fluxes, water fluxes, temperature, salinity, wind stress, and wind speed (Table 1). Conversely, our interannual simulation was made online, and it was made with daily to weekly forcing for the same fields. Both discontinuities produce an initial shock and a drift in our interannual results. To evaluate the impact of these two effects, we repeated our interannual simulation twice, using the end of the first simulation (in 1993) to reinitialize the second (in 1979). After 1980, the interannual variability of the two simulations was the same, an indication that the initial shock and the drift do not affect the interannual results

[*Le Quéré*, 1999]. To remove the average seasonal cycle, we subtracted, for each month during 1979 through 1997, the monthly average from the 1980 to 1993 period, during which the surface forcing remained from the same source (Table 1). We refer to the resulting deseasonalized time series as the interannual variability or the anomaly.

3. Results

3.1. Dynamic Response

In the equatorial Pacific, the observed SSTs [*Reynolds and Smith*, 1994] are 3.5°C colder in the east than in the west (Figure 2). The observed 20°C isotherm depth (D20) [*Hayes et al.*, 1991], which approximately indicates the depth of the upper thermocline, is also nearly 120 m shallower in the east. Modeled temperatures are in reasonable agreement with the observations, particularly toward the end of the simulation, when the forcing is more accurate because more observations were assimilated by ECMWF and NCEP/NCAR reanalysis. Nevertheless, when averaged over the 19 years of the simulation, modeled SSTs are too cold by 0.5 to 1.0°C, except around 95°W, where they agree with the observations. For the same period, modeled D20s agree with the observations at 95°W, but between 140°W and 110°W, D20s are deeper than observed by 8 to 25 m (Figure 2). Observed SSTs rise and the observed D20 deepens throughout the central and eastern equatorial Pacific during the El Niños of 1982-1983, 1986-1987, 1991-1992, 1993, 1994, and 1997-1998 (Figure 2). The amplitude and phase of the modeled SST and D20 anomalies agree well with the observations.

In the Southern Ocean at 57°S, the mean modeled SST of 2.6°C also agrees with observations but the amplitude of the modeled SST anomalies are smaller than observed by a factor of 2 (Figure 3). The agreement between the model and observations is better toward the end of the simulation when observed SST anomalies are smaller. In both the model and the observations, the SST anomalies propagate eastward around the globe approximately every 8 to 10 years [*White and Peterson*, 1996]. Cold SST anomalies are in phase with deep mixed layer anomalies. The amplitudes of the anomalies in modeled SSTs and mixed layer depth are largest in the Pacific sector of the Southern Ocean, where they reach values of ±0.5°C (±1.0°C in the observations) and ±50 m, respectively. In that region, the mean mixed layer depth reaches 300 m in winter.

In the North Atlantic Ocean, the mean modeled SST and SST anomalies generally agree with the observations at the oceanographic station India near Iceland

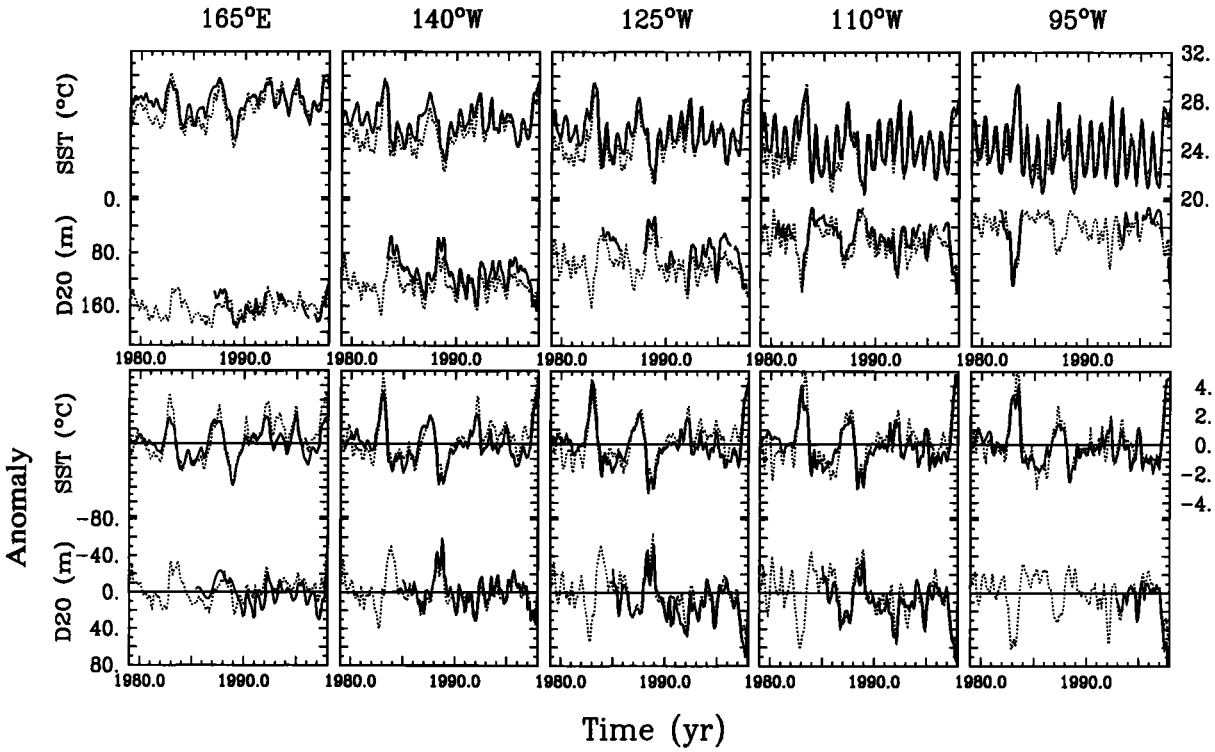

Figure 2. Time series of observed (solid line) and modeled (dotted line) sea surface temperature (SST) and the depth of the 20°C isotherm (D20) on the equator at 165°E, 140°W, 125°W, 110°W, and 95°W, showing (top) SST and D20 values and (bottom) SST and D20 anomalies from the mean seasonal cycle. The axis of the D20 is reversed. SST observations are from *Reynolds and Smith* [1994], and D20 values are computed from Tropical Atmosphere Ocean (TAO) temperature profiles [*Hayes et al.*, 1991]. The chosen locations correspond to the longest TAO moorings.

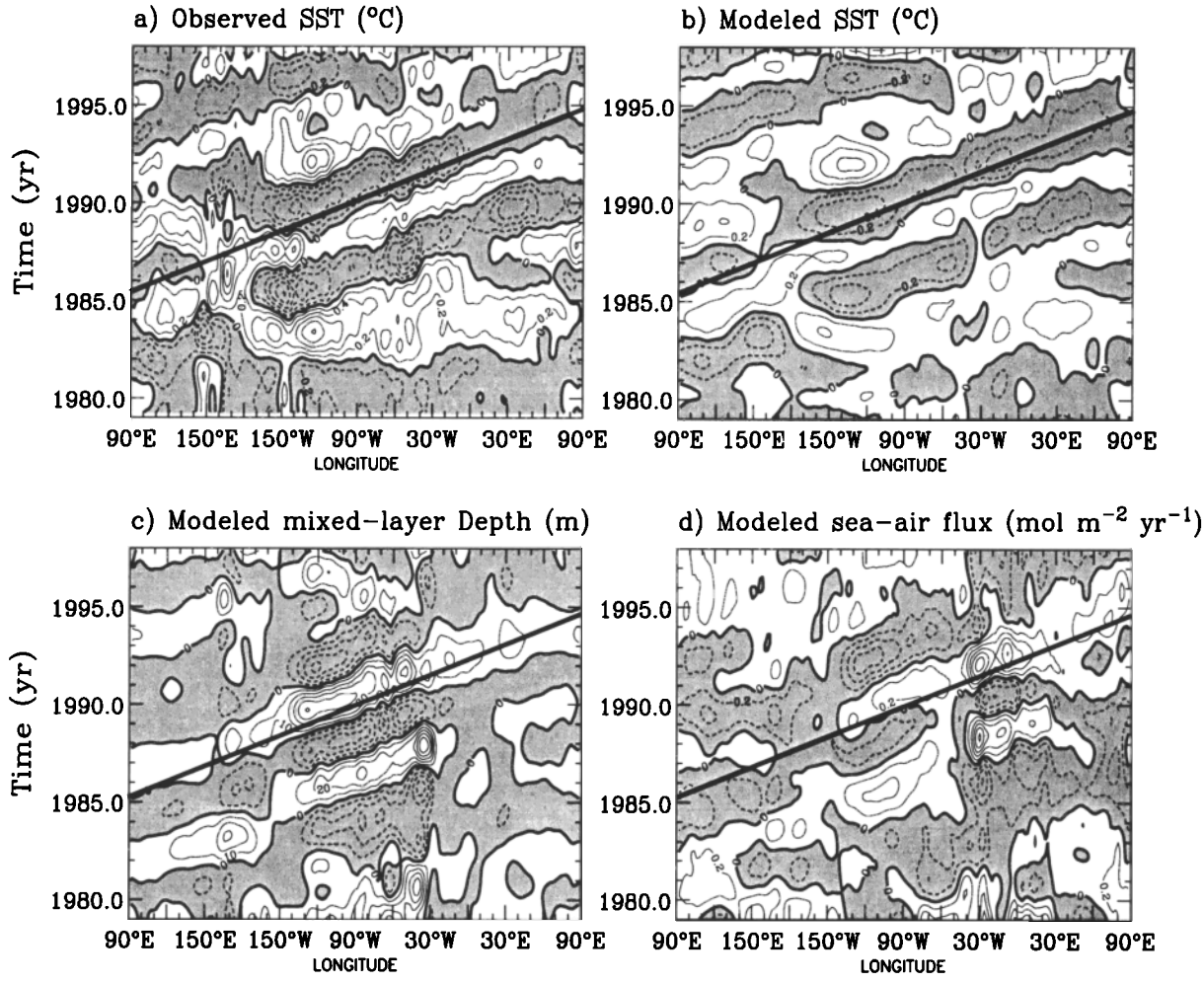

Figure 3. Interannual anomalies at 57°S of (a) observed SST from *Reynolds and Smith* [1994] (contours every 0.2°C), (b) modeled SST, (c) modeled mixed layer depth (contours every 10 m), and (d) modeled sea-air CO_2 flux (contours every 0.2 mol m^{-2} yr^{-1}). Both data and model results are filtered with a low-pass filter [*Thoning et al.*, 1989] to remove frequencies above 1 year^{-1} and smoothed using 6° of longitude, similar to the filtering options of *White and Peterson* [1996]. The thick solid line is for reference and is identical on all plots.

(59°N, 19°W) and at the Azores (39°N, 28°W) (Figure 4). SST anomalies are $\sim \pm 0.5$°C with mean values of 10° and 18°C, respectively. They vary approximately in phase with the North Atlantic Oscillation (NAO) index, i.e., the normalized atmospheric pressure difference between the Azores and Iceland [*Hurrell*, 1995]. Cold SST anomalies are in phase with deep mixed layer anomalies at Iceland. However, at the Azores, anomalies in the mixed layer depth show no systematic correlation with either the SST anomalies or the NAO. Mixed layer depth anomalies reach ±20 m, whereas the mean mixed layer depth is 610 m at Iceland and 165 m at the Azores during winter months.

3.2. Surface Oceanic pCO_2 in the Equatorial Pacific Ocean

To evaluate the simulated fluxes, we compared the modeled and observed sea-air pCO_2 difference (ΔpCO_2) in the equatorial Pacific between 15°S and 15°N, a region where many observations are available. The modeled ΔpCO_2 includes the anthropogenic contribution as described in section 2.2. The observational database [*Boutin and Etcheto*, 1997] covers most oceanic pCO_2 measurements made in this region and has been extended to 1979-1996 period, including data from *Feely et al.* [1987], *Weiss et al.* [1992], *Inoue and Sugimura* [1992], *Lefèvre and Dandonneau* [1992], *Wong et al.* [1993], *Murphy et al.* [1994], *Dandonneau* [1995], *Feely et al.* [1995], *Ishii and Inoue* [1995], *Wanninkhof et al.* [1996], *Coale et al.* [1996], *Archer et al.* [1996], and *Feely et al.* [1999]. We aggregated these data into bins corresponding to monthly averages over the model grid.

The observed averaged ΔpCO_2 for the area between 4°S and the equator increases from near zero in the western equatorial Pacific to ~85 μatm near 150°W, from 150°W to 120°W, observed ΔpCO_2 remains at

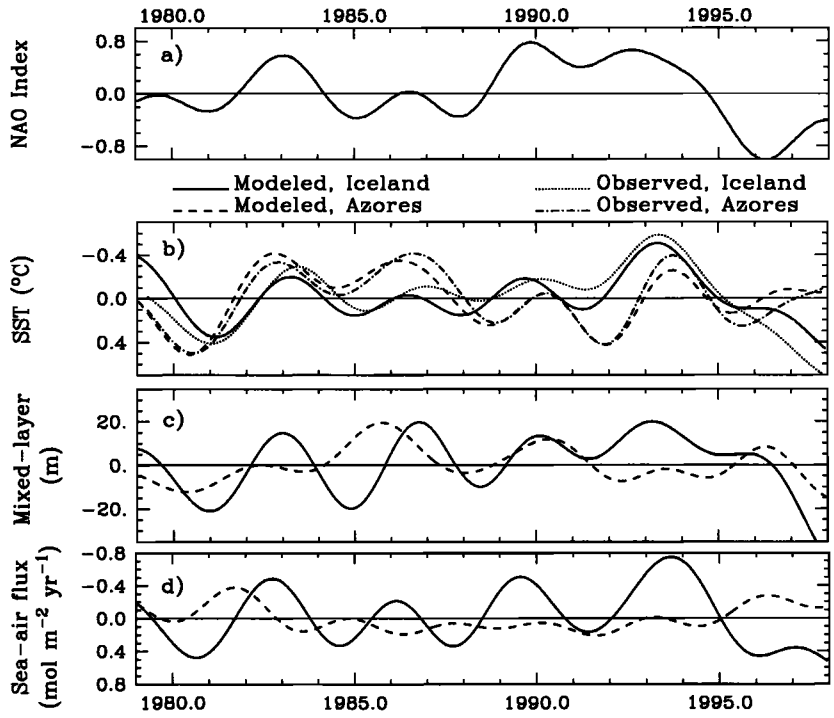

Figure 4. Interannual anomalies in the North Atlantic of (a) the North Atlantic Oscillation (NAO) index [*Hurrell*, 1995], (b) the modeled and observed SST (°C) [*Reynolds and Smith*, 1994], (c) the mixed layer depth (m), and (d) the sea-air flux (mol m^{-2} yr^{-1}). The solid lines in figures 4b-4d are results at station India, near Iceland (59°N, 19°W); dashed lines are results for the Azores (39°N, 28°W). The data and model results are filtered to remove frequencies above 1 year^{-1} [*Thoning et al.*, 1989]. The axis for the SST and CO_2 flux were reversed to illustrate their relationship with the NAO.

~85 μatm and increases to values between 100 and 120 μatm farther eastward (Figure 5 and Plate 1). Modeled ΔpCO_2 is also near zero in the western equatorial Pacific; however, when moving eastward of 165°W, modeled ΔpCO_2 begins to diverge from the observations, reaching values in the central and eastern basin that are from 30 to 80 μatm too low. Over the 1960-1996 period, the observed pCO_2 in the ocean increased at a rate between 80 and 122% that of the atmosphere in the central equatorial Pacific, when uncertainties in the measurement are taken into account [*Goyet and Peltzer*, 1994; *Feely et al.*, 1999]. In the same region, the modeled pCO_2 in the ocean increased at 90% of the atmospheric CO_2, which is within the limits of the observations. The agreement between the observed and modeled increase in pCO_2 is a consequence of the reasonable representation of the equatorial undercurrent and shallow equatorial upwelling in OPA. The residence time of surface water in that region seems therefore in agreement with observations. Other coarse-resolution OGCMs generally upwell waters from the deep ocean, which is in conflict with the observations [*Aumont et al.*, 1999].

In the equatorial Pacific, there are enough observations to compute an observed standard deviation for ΔpCO_2. Many locations have been revisited. The number of measurements at each revisited site varied between 2 and 24 (Plate 1e). We only kept the sites that were visited four times or more (506 sites). The observed standard deviation provides an indication of the variability in ΔpCO_2. High variability in ΔpCO_2 is observed in the western and in the eastern equatorial Pacific; low variability is observed in the central basin (Plate 1b). The magnitude of the standard deviation from 4°S to 4°N averages to 28, 18, and 32 μatm for the western (west of 165°W), central (165°W-120°W), and eastern basins (east of 120°W), respectively. The mean standard deviation is 25 μatm.

The modeled standard deviation of ΔpCO_2 in the equatorial Pacific also shows high variability in the western and eastern basin and low variability in the central basin, but the amplitude of the variability is underestimated, especially in the eastern equatorial Pacific (Plate 1d and 1f). The averaged modeled standard deviation, when the model is sampled as the observations, is 21 (-7), 10 (-8), and 17 (-15) in the western, central, and eastern basins, respectively, for a mean value of 16 μatm (-36%). The correlation r between the observed and modeled standard deviation (Plate 1b and 1d) is 0.47. The amplitude and horizontal distribution of the modeled standard deviation are similar when using all model grid points or when sampling the model output,

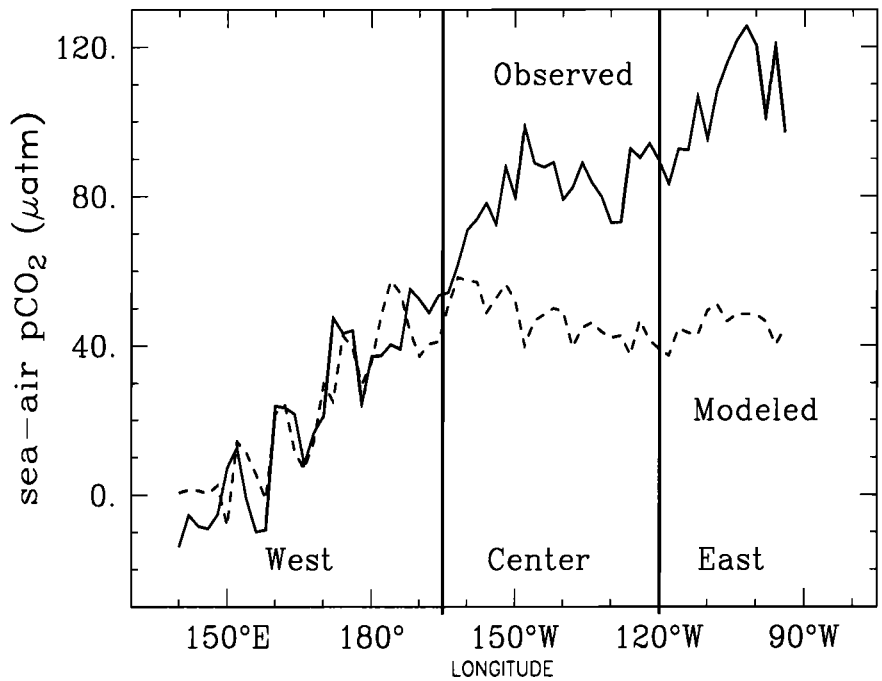

Figure 5. Sea-air pCO_2 (ΔpCO_2) in μatm averaged between 4°S and the equator for the observations (solid line) and the model sampled at the observation sites (dashed line). This region offers the densest data coverage [*Boutin and Etcheto*, 1997] and includes data from *Feely et al.* [1987], *Weiss et al.* [1992], *Inoue et al.* [1992], *Lefevre and Dandonneau* [1992], *Wong et al.* [1993], *Murphy et al.* [1994], *Dandonneau* [1995], *Feely et al.* [1995], *Ishii and Inoue* [1995], *Wanninkhof et al.* [1996], *Coale et al.* [1996], *Archer et al.* [1996], and *Feely et al.* [1999].

an indication that the number of observations is sufficient to perform this analysis (Plate 1d and 1f). The model results can be used to unravel the importance of interannual versus seasonal variability: interannual variability in ΔpCO_2 is responsible for > 80% of the total variance over most of the equatorial Pacific between 10°S and 10°N, maximum values exceed 95% in the central and western basin, and minimal values reach 45% in the eastern sector around 5°N.

3.3. Variability in Sea-Air Flux of CO_2

The modeled global flux of CO_2 from 1979 through 1997 varied by ±0.5 Pg C yr^{-1} for monthly averages (Figure 6) and by ±0.4 Pg C yr^{-1} for annual averages (Figure 1). The standard deviation of modeled CO_2 flux over the same period was 0.2 Pg C yr^{-1}. About 70% of the variance of the global flux originates from the equatorial Pacific (Figure 7). In the equatorial Pacific, during the El Niño events of 1982-1983, 1986-1987, and 1997-1998 and from 1990 through 1994, the direction of the interannual flux anomaly is from the atmosphere to the ocean (that is, the ocean gains CO_2). Conversely, the total CO_2 flux (not the anomaly) in the same region is always in the opposite direction, from the ocean to the atmosphere. The magnitude of the equatorial Pacific's CO_2 source to the atmosphere is 0.4 Pg C yr^{-1} for the 15°S to 15°N region, when averaged over 1979 to 1997. In comparison, the estimated CO_2 source to the atmosphere based on observations is 0.6 Pg C yr^{-1}, on average over approximately the same period and region [*Feely et al.*, 1997, 1999]. In our model, the equatorial Pacific source to the atmosphere was reduced to nearly zero during El Niño events, while during cold events, it reached 0.8 Pg C yr^{-1} (Figure 6). The propagation of the flux anomalies in the equatorial Pacific is from west to east, as shown by the correlation between the two regions, which is maximum (r=0.55) when the flux from the western basin leads that of the eastern basin by 3 months. Furthermore, relative to the Southern Oscillation Index (SOI), the modeled flux anomaly in the equatorial Pacific has a maximum correlation (r=0.59) when the flux lags the SOI by 3-4 months (Figure 7).

Although other regions do not exhibit as much variability as the equatorial Pacific, when added together, they account for 30% of the global variance in sea-air flux (Figure 6). Next in areal extent is the Southern Ocean. At 57°S (Figure 3), the flux anomaly is directed from the ocean to the atmosphere when the SSTs are cold and the mixed layer is deep, which indicates the dominance of dynamic processes at that latitude [*Le Quéré*, 1999]. The variability in sea-air flux follows the Antarctic Circumpolar Wave (ACW). Its maximum amplitude is ±0.8 mol m^{-2} yr^{-1} around the Drake passage, where the mixed layer varies the most.

Although the North Atlantic is a region where interannual variability in ocean dynamics is well docu-

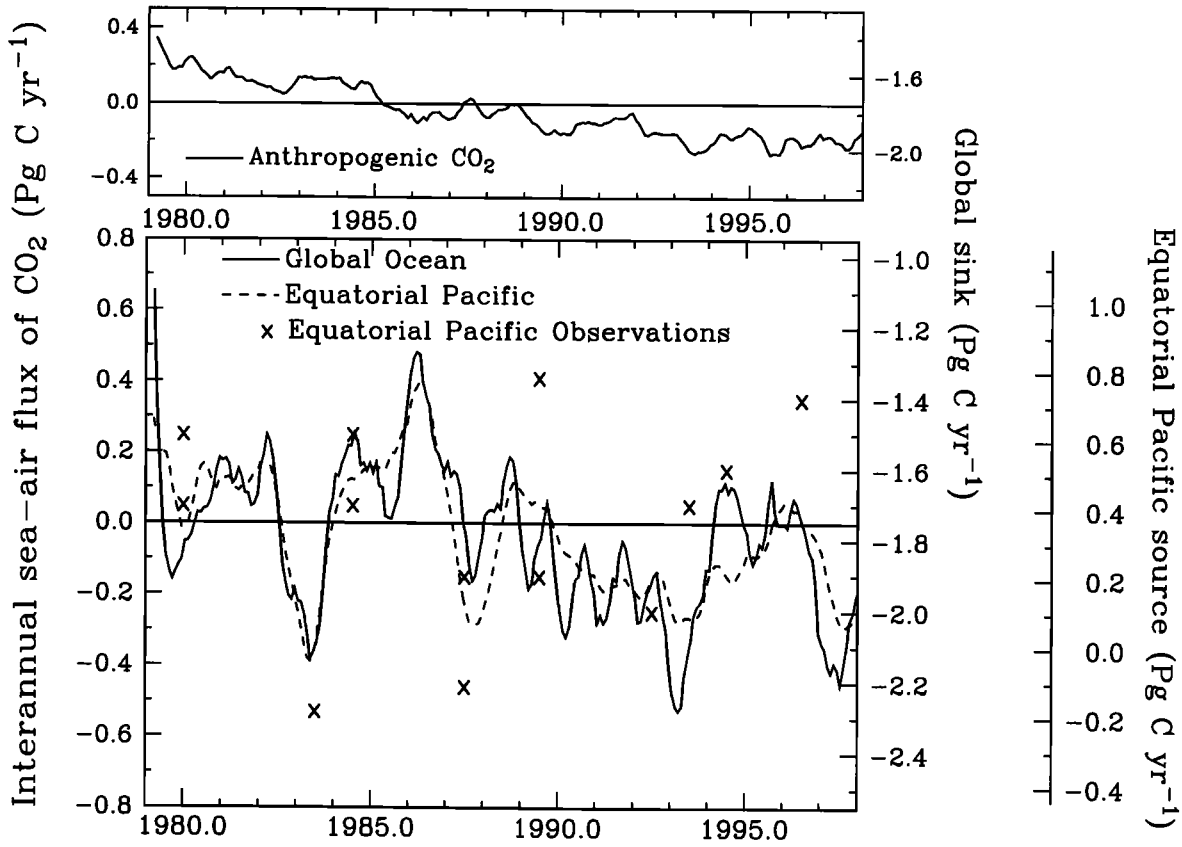

Figure 6. Anomalies of sea-air flux of CO_2 (left axis) as well as net flux (right axis), in Pg C yr^{-1} for the global ocean (solid line) and the equatorial Pacific (dashed line). On average in the model, the global ocean is a sink of 1.8 Pg C yr^{-1}, whereas the equatorial Pacific is a source of 0.4 Pg C yr^{-1}. The anthropogenic anomaly and the net anthropogenic component are shown separately (top) but are also included at bottom. The equatorial observations are the same as in Figure 1. A 5 month running average was applied to the results after the mean seasonal signal was removed. Positive values of the flux are from ocean to atmosphere.

mented, there is little contribution of that region to the global variability in sea-air flux (Figure 7). However, local variability is important. Maximum amplitudes in the model reach ±0.6 mol m^{-2} yr^{-1} (Figure 4). The interannual sea-air flux of CO_2 at Iceland is strongly correlated with the NAO index. The flux anomaly is from atmosphere to ocean when SSTs are cold and the mixed layer is deep, an indication of the dominance of thermodynamic processes. On the contrary, the flux anomaly at the Azores is generally opposed in sign from that at Iceland from 1983 onward, where changes in the mixed layer depth are equally as important as thermodynamics.

4. Discussion

This discussion focuses on evaluating the model results. More specifically, we try to test, based on observations, whether our estimated interannual variability in the air-sea CO_2 flux has approximately the correct amplitude. Most of the discussion will focus on possible sources of error.

4.1. Dynamic Response

The agreement between the model results and the observations for the amplitude of the interannual variabilities in SST and D20 in the equatorial Pacific (Figure 2) suggests that the model and surface forcing are adequate for interannual simulations. Agreement is especially good toward the end of the simulation when an increased number of observations were assimilated by ECMWF and NCEP/NCAR to produce the wind stress and fluxes fields [*Uppala*, 1997]. Yet, even at the end of the simulations, the modeled D20 is too deep in the central equatorial Pacific. Thus the vertical gradient of temperature in the upper thermocline is too weak (Figure 2). This problem appears to derive from inaccuracies in the modeled equatorial undercurrent in the center of the basin. The magnitude of the discrepancy between the modeled and observed D20 reaches 25 m, which is relatively small. The problem is localized in the central Pacific.

In the Southern Ocean at 57°S, the eastward propagation of SSTs and mixed layer depth anomalies are

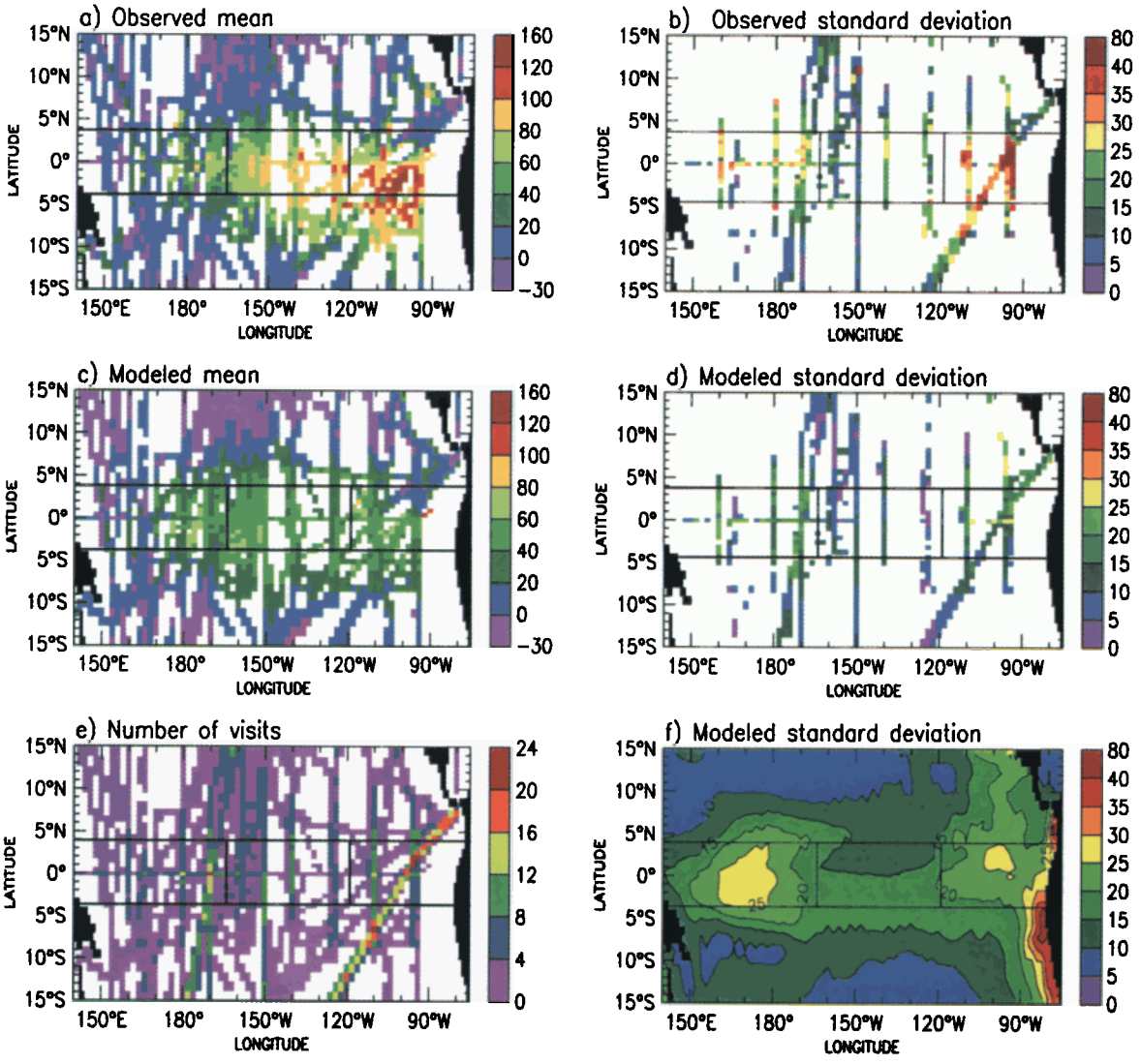

Plate 1. (a) Mean and (b) standard deviation of ΔpCO_2 in μatm for the observations and (c) mean and (d) standard deviation for the model sampled like the observations. (e) Number of visits at each station. The standard deviation is computed using only the locations visited four times or more, where the number of visits is computed by averaging the total number of observations in each model grid box of $\sim 0.5°$ of latitude by 2° of longitude and monthly averages. (f) Modeled standard deviation using all grid boxes at all times. The source of the database is cited in Figure 5. The black lines are the same in all panels and separate the western, central, and eastern basins as described in the text.

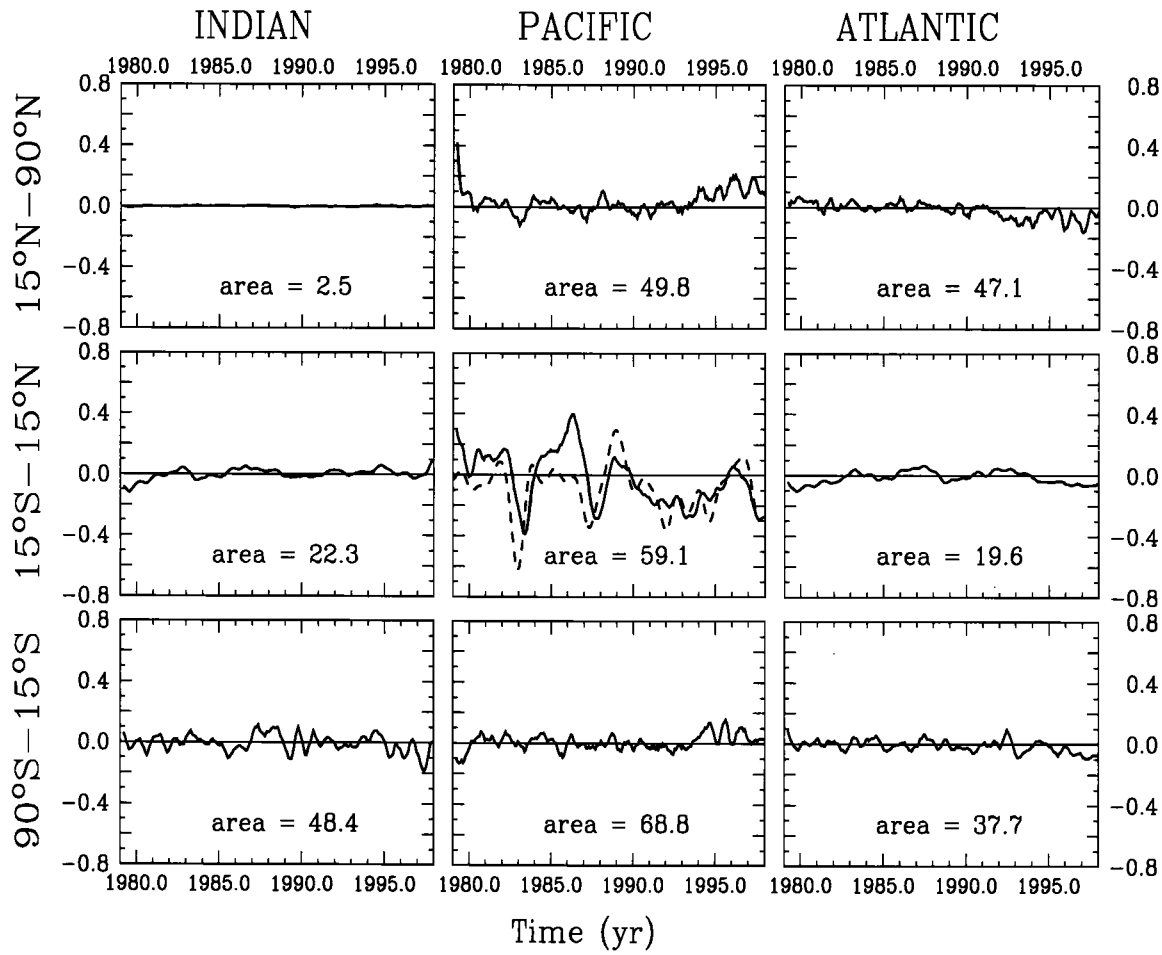

Figure 7. Modeled sea-air flux anomalies in Pg C yr^{-1} (solid line). (left to right) Indian, Pacific, and Atlantic Oceans and regions (top) north of 15°N (top), (middle) 15°S to 15°N, and (bottom) south of 15°S. The dashed line is the Southern Oscillation Index (SOI). Regional areas are given in million km^2.

driven by the ACW (Figure 3), which *White and Peterson* [1996] detected in meridional wind stress, SST, sea level pressure, and sea ice extent. The model ocean responds to variations in surface fluxes and wind stress by generating variations in the depth of the mixed layer. However, the amplitude of modeled SST anomalies is half that observed. This weaker amplitude results from (1) the semidiagnostic forcing (restoring of T and S toward climatological observations below the mixed layer), which dampens variability below the mixed layer, except near the coast at Drake passage; (2) inaccuracies in the wind stress field over the Southern Ocean due to sparseness of data; and (3) the initial conditions, which are inconsistent with the observed ACW pattern in 1979. The agreement between modeled and observed SST anomalies is better toward the end of the simulation, when the winds are more accurate and after anomalies had already propagated once around the Southern Ocean. The passage of the ACW, with its associated change in SST and mixed layer depth, also substantially affects the regional sea-air flux by modifying the rate of gas exchange, vertical mixing, and biological export of carbon.

4.2. Surface Oceanic pCO_2 in the Equatorial Pacific Ocean

The model results agree spatially with observations, but the variability is 36% less than observed over the whole equatorial Pacific. The modeled variability of ΔpCO_2 may be generally too low partly because the model neglects certain time and length scales. For instance, the model does not account for the diurnal cycle and for mesoscale instabilities. The diurnal cycle in surface pCO_2 in the equatorial Pacific was measured in fall 1992 and had a standard deviation of 4-8 μatm [*Goyet and Peltzer*, 1997; *Feely et al.*, 1997]. Mesoscale instabilities can also produce significant variations in surface pCO_2. One event reported by *Feely et al.* [1997] caused ΔpCO_2 to decrease by 33 μatm in fall 1992. However, the neglect of higher frequencies by the model, while it could account for most of the 7 and 8 μatm underestimated variability in ΔpCO_2 in the western and central

basin, can hardly explain all of the 15 μatm underestimate in the eastern basin.

The difficulties in modeling the variability in ΔpCO_2 appear related to the difficulties in modeling the mean state of tracers (Figure 5 and Plate 1). Ocean dynamics cannot be responsible for the underestimated ΔpCO_2 in the eastern basin. Indeed, ocean circulation is reasonably well simulated in the eastern basin, where the modeled ΔpCO_2 is farthest from observations. However, in the central basin, inaccuracies in ocean dynamics persist. The impact of these inaccuracies is hard to quantify. Nevertheless, the agreement between the observed and modeled increase in anthropogenic pCO_2 in the central basin indicates that the residence time of surface water in that region is reasonable. Therefore other causes must come into play. Uncertainties in the gas exchange cannot account entirely for the difference between modeled and observed ΔpCO_2 either: we made a sensitivity study, discussed below, which suggests that ΔpCO_2 would increase by only 5 μatm if we had used the *Liss and Merlivat* [1986] gas exchange formulation instead of *Wanninkhof* 's [1992] in our standard run. Finally, *Wanninkhof et al.* [1999] recommend the use of dissociation constants from *Mehrbach et al.* [1973], because other constants can cause a systematic bias of up to 30 μatm in the estimated pCO_2. *Wanninkhof et al.* [1999] have not, however, tested the constants of *Edmond and Gieskes* [1970], which we use. Furthermore, such systematic bias cannot explain our difficulties in modeling the east-west gradient of ΔpCO_2. Another explanation is needed.

Thus we turn to the biological pump as a possible cause of the underestimated variability in ΔpCO_2. Our model's underestimate of ΔpCO_2 in the central and eastern equatorial Pacific could be caused by our model's export production that is too high (up to 20 mmol C m^{-2} d^{-1}), whereas data-based estimates are generally below 10 mmol C m^{-2} d^{-1} [*Jianrong and Quay*, 1997]. The latter contain both seasonal as well as interannual variability [*Foley et al.*, 1997]. Our overestimated biological production is thus too high, a consequence of the absence of DOC, grazing by zooplankton, and iron limitation in HAMOCC3 [*Six and Maier-Reimer*, 1996; *Aumont*, 1998; *Stoens et al.*, 1998; *Coale et al.*, 1996]. Further supporting evidence that excess biological productivity is the culprit comes from the model's surface concentration of PO_4^{3-}, which is too low by ~20% in the equatorial Pacific.

The evidence shows that our mean biological export production is too large in the central and especially in the eastern equatorial Pacific. How does this affect the variability in pCO_2? A preliminary study, using Sea-viewing wide-field-of-view Sensor (SeaWiFS) chlorophyll [*Murtugudde et al.*, 1999], shows that the decrease in export production caused by the 1997-1998 El Niño event could be 100% overestimated by the model in the eastern equatorial Pacific, which would partly cancel the variability driven by ocean dynamics (see section 4.3). However, the model reproduced both the reduction in export production by 20% over the rest of the equatorial Pacific and its increase by 40% in the eastern Indian Ocean [*Le Quéré*, 1999]. Thus the mean concentration of tracers must be simulated correctly in order to properly simulate variability. The importance of the eastern equatorial Pacific for the global fluxes of CO_2 will be discussed in section 4.4.

The western maximum in standard deviation of ΔpCO_2 is located at the eastern edge of the warm pool, i.e., roughly between 160°E and 160°W. This region also corresponds to the eastern edge of the barrier layer, a stratified water column of homogeneous temperature which lies under the mixed layer and whose thickness can exceed 20 m [*Ando and McPhaden*, 1997]. The depth and location of the barrier layer also show strong interannual variability related to El Niño events [*Vialard and Delecluse*, 1998]. During El Niño events, fresh warm waters originating from the western equatorial Pacific propagate eastward through equatorial jets [*Roemmich et al.*, 1994]. These jets were observed to affect local pCO_2 and salinity in the western basin [*Feely et al.*, 1995; *Inoue et al.*, 1996]. *Fushimi* [1987] also showed that a strong correlation exists between pCO_2 and salinity in the same area. Our model shows such a relationship between variations in ΔpCO_2 and salinity in the western equatorial Pacific.

4.3. Component Analysis

Volk [1989] pointed out that interannual variations in the sea-air flux of CO_2 result from a balance of processes driven by ocean biology, dynamics, and thermodynamics. In this section, we study the relative role of these processes by analyzing modeled variability in the equatorial Pacific between 15°S and 15°N, over the top 50 m of the ocean.

The flux of CO_2 results from the product of a gas exchange coefficient and ΔpCO_2. Direct measurements are available for ΔpCO_2 but not for the gas exchange coefficient. Gas exchange must be estimated indirectly and has large uncertainty [*Boutin and Etcheto*, 1997]. Thus estimates of sea-air flux based on observed ΔpCO_2 are encumbered by this large uncertainty. In contrast, models give flux estimates that vary less with the gas exchange coefficient, because changing the gas exchange coefficient also affects modeled ΔpCO_2. *Verschell* [1996], using a model of the equatorial Pacific between 3°S and 3°N, showed that the interannual sea-air flux anomaly changed by $\sim \pm 10\%$ between two simulations where the gas exchange coefficient was fixed versus that where it was left to vary interannually. A sensitivity study made with our model showed that when gas exchange coefficient was increased by 300%, the sea-air flux increased by 70%, the standard deviation in sea-air flux increased by 150%, and ΔpCO_2 decreased by 60%. Extrapolating linearly, a 50% reduction in the gas exchange coefficient should result in a 12% reduction in the sea-air flux, a 25% reduction in its standard deviation, and a 10% increase in ΔpCO_2. Another sensitivity study without chemical enhancement (i.e., using *Wanninkhof* 's [1992] equation (3) instead of equation (8)) scarcely affected the standard deviation in the modeled

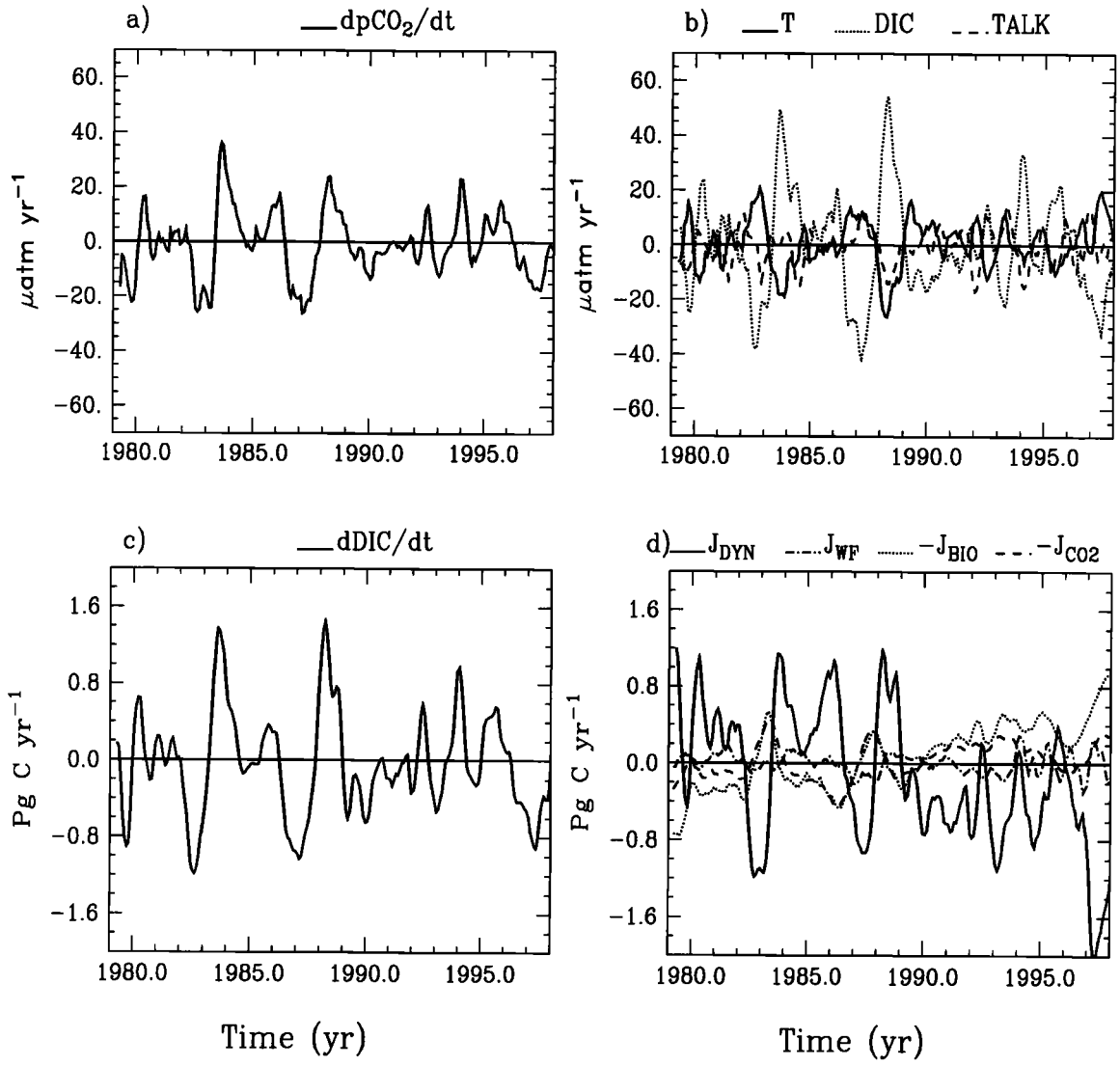

Figure 8. Component analysis for all terms of equations (5) and (3a) averaged over the equatorial Pacific Ocean between 15°S and 15°N and 50 m depth: (a) $dpCO_2/dt$, (b) $\partial pCO_2/\partial T\ dT/dt$ (solid line), $\partial pCO_2/\partial \mathrm{DIC}\ d\mathrm{DIC}/dt$ (dotted line), and $\partial pCO_2/\partial \mathrm{TALK}\ d\mathrm{TALK}/dt$ (dashed line), (c) $d\mathrm{DIC}/dt$ and ,(d) J_{DYN} (solid line), J_{WF} (dash-dotted line), $-J_{\mathrm{BIO}}$ (dotted line), and $-J_{CO_2}$ (dashed line).

flux and increased oceanic pCO_2 in the equatorial Pacific by 5 μatm, on average.

Besides gas exchange, the sea-air flux of CO_2 is affected by ΔpCO_2. Factors affecting oceanic pCO_2 include DIC, temperature T, TALK, and salinity S. Their effects on pCO_2 can be written as

$$\frac{dpCO_2}{dt} = \frac{\partial pCO_2}{\partial \mathrm{DIC}}\frac{d\mathrm{DIC}}{dt} + \frac{\partial pCO_2}{\partial T}\frac{dT}{dt} + \frac{\partial pCO_2}{\partial \mathrm{TALK}}\frac{d\mathrm{TALK}}{dt} + \frac{\partial pCO_2}{\partial S}\frac{dS}{dt} \quad (5)$$

The left hand term ($dpCO_2/dt$) is the sum of all effects (Figure 8a). In the first right-hand term, DIC is affected by ocean dynamics, water fluxes, biological sources and sinks, and the sea-air flux of CO_2 (equation (3a)). In the second term, temperature is affected by ocean dynamics and the heat flux. In the third term, TALK is affected by variability in surface salinity (equation (4)). For the fourth term, the sensitivity of pCO_2 to salinity is negligible. It is not considered further. Figure 8b shows that it is the changes in DIC that have the largest impact on pCO_2. The temperature effect opposes the effect of DIC but has about half its amplitude.

Variability in DIC of the mixed layer ($d\mathrm{DIC}/dt$) exceeds ± 1.2 Pg C yr^{-1} when integrated over the surface 50 m of the equatorial Pacific Ocean between 15°S and 15°N (Figure 8c). The dominant processes controlling changes in $d\mathrm{DIC}/dt$ is the ocean transport of DIC, J_{DYN}, which includes vertical and horizontal transport by advection and diffusion. The transport of DIC by

advection and diffusion exhibits variability related to El Niño events. J_{WF}, the dilution and concentration of DIC caused by freshwater fluxes, is relatively small and noisy. However, in sensitivity tests when ECMWF water fluxes were used, this term became dominant because of the excessive and unrealistic variability of these fluxes. The other processes affecting DIC, the biological sources and sinks J_{BIO} and the sea-air flux J_{CO_2}, are each about a third of the magnitude and oppose J_{DYN}.

In summary, our calculations infer that it is ocean dynamics that control the variability in DIC in the equatorial Pacific, even though the biological pump and the gas exchange are significant. Therefore since DIC is controlled mostly by changes in ocean dynamics and DIC is mostly responsible for changes in pCO_2, then changes in ocean dynamics are the main mechanism driving the modeled variability in pCO_2 in the equatorial Pacific, in agreement with the conclusions of *Archer et al.* [1996].

4.4. Variability in Sea-Air Flux of CO_2

The variability in the global sea-air flux of CO_2 in our model is ± 0.4 Pg C yr^{-1} when averaged annually. Only 30% of the global variance in sea-air flux originates from outside the equatorial Pacific. The relatively large importance of the equatorial Pacific compared to the rest of the ocean in our model is caused by three factors. First, the equatorial Pacific is the only region where interannual variability occurs in phase over the whole basin. Anomalies in other basins, such as those associated with ACW and NAO, as well as with oscillations in the North Pacific and South Atlantic, have dipoles of positive and negative anomalies, which partly cancel one another. Second, the equatorial Pacific is a region where dynamic processes dominate, in agreement with observations [*Archer et al.*, 1996]. Over most of the rest of the ocean, the thermodynamic, dynamic, and biological processes have amplitudes that are close to one other and partly cancel. Observations from the Southern Ocean provide a good example [*Louanchi et al.*, 1999]. Third, our dynamic and biology models likely underestimate the variability at high latitudes. The last of these three factors is an artifact of our model. However, even if ocean dynamics or biology induces greater variability than suggested by our model, which is likely, those two factors would still dampen one another. Thus high latitudes are unlikely to be a major source of global variability in atmospheric CO_2.

About 70% of the model's global variance originates in the equatorial Pacific. To evaluate our variability estimates there, we compared our results with a variety of observations. On one hand, modeled and observed anomalies of SST and D20 generally agree in amplitude and in phase. Furthermore, 64% of the amplitude of the standard deviation in ΔpCO_2 is reproduced by the model. On the other hand, the mean ΔpCO_2 is 30 to 80 μatm too low in the eastern basin, where the averaged standard deviation is underestimated by 15 μatm. To quantify the effect of our underestimated variability in ΔpCO_2 in the eastern equatorial Pacific, we can compare our flux estimate with data-based estimates [*Keeling and Revelle*, 1985; *Smethie et al.*, 1985; *Takahashi et al.*, 1986; *Feely et al.*, 1987; *Volk*, 1989; *Inoue and Sugimura*, 1992; *Wong et al.*, 1993; *Feely et al.*, 1995, 1997, 1999]. Modeled and observed estimates can differ by up to 0.4 Pg C yr^{-1}. However, the maximum observed variability is ± 0.5 Pg C yr^{-1} (year 1989-1992), 20% greater than the maximum model estimate (Figure 6). This small difference is due to the small surface area covered by the eastern equatorial Pacific (25%), which harbors most of the discrepancy between our model estimates and the observations (Plate 1b and d). Furthermore, the modeled variability in CO_2 fluxes for the region from 5°S to the equator agrees in phase and in amplitude with those of *Boutin et al.* [1999], who estimated the Pacific sea-air fluxes over that region using the observed relationship between pCO_2 and SST [*Le Quéré*, 1999]. Therefore, in spite of our underestimate of the variability in ΔpCO_2 in the eastern equatorial Pacific, our estimated variability in the flux of CO_2 is in general agreement with that observed (to ± 0.1 Pg C yr^{-1}). That difference is relatively small compared with differences between ocean- and atmosphere- based estimates (Figure 1).

In the equatorial Pacific, our model estimates a flux of CO_2 from ocean to atmosphere that varies between 0 and 0.8 Pg C yr^{-1}. The lowest fluxes occur during El Niño warm events. Yet atmospheric CO_2 growth rate, on the contrary, increases by 2-4 Pg C yr^{-1} during El Niño warm events, with the exception of the early 1990s [*Keeling et al.*, 1989; *Conway et al.*, 1994; *Keeling et al.*, 1995]. Therefore the sea-air flux cannot explain changes in atmospheric growth rate caused by El Niño events. On the other hand, it has been observed that at the onset of El Niño warm events, the atmospheric growth rate decreases slightly before it increases (by $\sim$0.3 μatm yr^{-1} or 0.6 Pg C yr^{-1}) [*Keeling and Revelle*, 1985; *Volk*, 1989; *Elliot et al.*, 1991]. According to our model, such a decrease could be caused by the sea-air flux, which lagged the onset of El Niño by only 3 months.

Finally, from 1991 through 1993, a large decrease of 1-2 Pg C yr^{-1} occurred in the atmospheric growth rate of CO_2. This decrease has been attributed to unknown consequences of the volcanic eruption of Mount Pinatubo in June 1991 [*Conway et al.*, 1994; *Sarmiento*, 1993]. Our model estimates a decrease of 0.2 Pg C yr^{-1} in the global sea-air flux of CO_2 originating entirely from the equatorial Pacific (Figure 6). This decrease accounts for $\sim$10% of the observed decline in atmospheric growth rate during 1991 through 1993. Our estimate is in relative agreement with the observed decrease in the equatorial Pacific of 0.3 to 0.6 Pg C yr^{-1}, estimated to account for 26% of the atmospheric decrease over 1992-1993 [*Feely et al.*, 1999]. The larger ocean sink of CO_2 during 1991-1994 is caused by the successive El Niño events of 1991-1992, 1993, and 1994 which reduced the

equatorial upwelling throughout this period. They are not directly related to the volcanic eruption of Mount Pinatubo.

5. Conclusions

The global variability of the sea-air flux of CO_2 (annually averaged) was ± 0.4 Pg C yr^{-1}. When added to our mean ocean sink of anthropogenic CO_2 of 1.8 Pg C yr^{-1}, that gives a range from 1.4 to 2.2 Pg C yr^{-1} for 1979 through 1997. The variability in sea-air flux has about a quarter of the amplitude of the atmospheric growth rate of CO_2 [*Keeling et al.*, 1989; *Conway et al.*, 1994; *Tans et al.*, 1996]. Thus exchange of the atmosphere with the terrestrial biosphere must control most of the atmospheric variability, a conclusion which supports other ocean-based estimates [*Winguth et al.*, 1994; *Lee et al.*, 1998; *Feely et al.*, 1987; *Inoue and Sugimura*, 1992; *Wong et al.*, 1993; *Feely et al.*, 1997; *Boutin et al.*, 1999; *Feely et al.*, 1999] but disagrees with the larger atmosphere-based estimates [*Keeling et al.*, 1995; *Francey et al.*, 1995; ?; *Joos et al.*, 1999] (Figure 1).

An evaluation of the model results in the equatorial Pacific shows that our interannual variability is in general agreement with that observed to ± 0.1 Pg C yr^{-1}. In spite of our efforts though, global evaluation of our model results is not possible. An analysis such as the one we did for the equatorial Pacific would not be appropriate outside the equatorial region, as the seasonal cycle is too large and hard to extract. Our global flux estimate therefore depends on the global variability in the winds and fluxes we used and on the validity of our model. For the surface forcing, we are totally dependent on the reanalyzed data by ECMWF and NCEP/NCAR. ECMWF provided good wind fields; however, their global water fluxes had unrealistically large interannual fluctuations and could not be used for that reason. Nevertheless, opposing positive and negative anomalies and opposing effects due to thermodynamic, dynamics, and biological processes in regions outside the equator mean that higher latitudes play a small role in global variability.

Future modeling efforts will explore interannual variability using a fully prognostic version of our dynamic model including isopycnal mixing, which should provide more realistic interannual predictions in frontal regions such as the Southern Ocean and on a decadal timescale. Furthermore, we will include a more sophisticated biological model which does a better job of reproducing the seasonal cycle at high latitudes, the vertical profile of TALK, and the mean ΔpCO_2 in the equatorial Pacific [*Aumont*, 1998]. To pursue this study, however, time series of carbon-related biogeochemistry, such as those of the Hawaiian Ocean Time-series (HOT) and Bermuda Atlantic Time-series Study (BATS) [*Karl et al.*, 1996; *Bates et al.*, 1996, 1998], are necessary, especially in the Southern Ocean, to understand the processes driving variability in those regions.

Studying interannual variability provides insight into how climatically driven changes affect the ocean carbon cycle. Indeed, some models have begun to predict consequences of future global warming, which include surface warming and freshening, reduction in the vertical transport of carbon, and reduction in the intensity of the biological pump [*Maier-Reimer et al.*, 1996; *Sarmiento and Le Quéré*, 1996; *Sarmiento et al.*, 1998; *Matear and Hirst*, 1999]. Similar processes operate at the interannual timescale. Yet, unlike simulations for future climate change, interannual simulations can be validated. More detailed model development and validation on the interannual timescale will also benefit those studying future climate change with similar models. Nevertheless, a good representation of the mean surface and subsurface concentration of carbon-related species (DIC, TALK, SST) is unavoidable for accurate model simulations of biogeochemical variability.

Acknowledgments. We appreciate detailed comments from N. Gruber, A. Winguth, and R. Feely. We thank J. Boutin, P. Ciais, P. Rayner, J. Sarmiento, J. Vialard, P. Delecluse, L. Memery, V. Garçon, and J. Etcheto for discussions during this project. We thank J. Boutin for providing the pCO_2 database and the following who have provided pCO_2 data: Y. Dandonneau, R. Feely, H. Inoue, M. Ishii, N. Lefèvre, P. Murphy, P. Nightingale, R. Wanninkhof, R. Weiss, and C. S. Wong. We are grateful to NCEP and NCAR for providing the flux data and ERS and ECMWF for providing the wind fields. Finally, we thank M.A. Foujols, M. Imbard, C. Levy, and C. Boone for their help in preparing model simulations. Figures were made with PMEL's program Ferret. C.L.Q. was supported by the French CNOUS and the EC Environment and Climate Programme (ENV4-CT95-0132). We thank the French CNRS/IDRIS and CEA-Grenoble for computing support. This is LSCE contribution 278.

References

Ando, K., and M. J. McPhaden, Variability of surface layer hydrography in the tropical Pacific Ocean, *J. Geophys. Res.*, *102*, 23,063–23,078, 1997.

Archer, D. E., T. Takahashi, S. Sutherland, J. Goddard, D. Chipman, K. Rodgers, and H. Ogura, Daily, seasonal and interannual variability of sea-surface carbon and nutrient concentration in the equatorial Pacific Ocean, *Deep Sea Res., Part II*, *43*, 779–808, 1996.

Aumont, O., Étude du cycle naturel du carbone dans un modèle 3D de l'océan mondial, Ph.D. thesis, Univ. Pierre et Marie Curie, Paris, 1998.

Aumont, O., J. C. Orr, D. Jamous, P. Monfray, O. Marti, and G. Madec, A degradation approach to accelerate simulations to steady-state in a 3-D tracer transport model of the global ocean, *Clim. Dyn.*, *14*, 101–116, 1998.

Aumont, O., J. C. Orr, P. Monfray, G. Madec, and E. Maier-Reimer, Nutrient trapping in the equatorial Pacific: The ocean circulation solution, *Global Biogeochem. Cycles*, *13*, 351–369, 1999.

Bates, N. R., A. F. Michaels, and A. H. Knap, Seasonal and interannual variability of oceanic carbon dioxide species at the U.S. JGOFS Bermuda Atlantic Time-series Study Site, *Deep Sea Res., Part II*, *43*, 347–384, 1996.

Bates, N. R., A. H. Knap, and A. F. Michaels, The effect of hurricanes on the local to global air-sea exchange of CO_2, *Nature, 395*, 58–61, 1998.

Blanke, B., and P. Delecluse, Low frequency variability of the tropical Atlantic ocean simulated by a general circulation model with mixed layer physics, *J. Phys. Oceanogr., 23*, 1363–1388, 1993.

Boutin, J., and J. Etcheto, Long-term variability of the air-sea CO_2 exchange coefficient: Consequences for the CO_2 fluxes in the equatorial Pacific Ocean, *Global Biogeochem. Cycles, 11*, 453–470, 1997.

Boutin, J., et al., Satellite sea surface temperature: a powerful tool for interpreting *in situ* measurements in the equatorial Pacific Ocean, *Tellus, Ser.B, 51*, 490–508, 1999.

Coale, K. H., et al., A massive phytoplankton bloom induced by an ecosystem-scale iron fertilization experiment in the equatorial Pacific Ocean, *Nature, 383*, 495–501, 1996.

Conway, T. J., P. P. Tans, L. S. Waterman, K. W. Thoning, D. R. Kitzis, K. A. Masarie, and N. Zhang, Evidence for interannual variability of the carbon cycle from the National Oceanic and Atmospheric Administration/Climate Monitoring and Diagnostics Laboratory Global Air Sampling Network, *J. Geophys. Res., 99*, 22,831–22,855, 1994.

Dandonneau, Y., Sea-surface partial pressure of carbon dioxide in the eastern equatorial Pacific (August 1991 to October 1992): a multivariate analysis of physical and biological factors, *Deep Sea Res., Part II, 42*, 349–364, 1995.

Edmond, J. M., and T. M. Gieskes, On the calculation of the degree of saturation of sea water with respect to calcium carbonate under *in situ* conditions, *Geochim. Cosmochim. Acta, 34*, 1261–1291, 1970.

Elliot, W. P., J. K. Angell, and K. W. Thoning, Relation of atmospheric CO_2 to tropical sea and air temperatures and precipitation, *Tellus, Ser.B, 43*, 144–155, 1991.

Enting, I. G., T. M. L. Wigley, and M. Heimann, Future emissions and concentrations of carbon dioxide: Key ocean/atmosphere/land analyses, *Tech. Rep. 31*, Div. of Atmos. Res., Commonw. Sci. and Ind. Res. Org., Melbourne, Victoria, 1994.

Feely, R. A., R. H. Gammon, B. A. Taft, P. E. Pullen, L. S. Waterman, T. J. Conway, J. F. Gendron, and D. P. Wisegarver, Distribution of chemical tracers in the eastern equatorial Pacific during and after the 1982-1983 El-Niño/Southern Oscillation event, *J. Geophys. Res., 92*, 6545–6558, 1987.

Feely, R. A., R. Wanninkhof, C. E. Cosca, P. P. Murphy, M. F. Lamb, and M. D. Steckley, CO_2 distributions in the equatorial Pacific during the 1991-1992 ENSO event, *Deep Sea Res., Part II, 42*, 365–386, 1995.

Feely, R. A., R. Wanninkhof, C. Goyet, D. E. Archer, and T. Takahashi, Variability of CO_2 distributions and sea-air fluxes in the central and eastern equatorial Pacific during the 1991-1994 El Niño, *Deep Sea Res., Part II, 44*, 1851–1867, 1997.

Feely, R. A., R. Wanninkhof, T. Takahashi, and P. Tans, Influence of El Ni no on the equatorial Pacific contribution to atmospheric CO_2 accumulation, *Nature, 398*, 597–601, 1999.

Foley, D. G., T. D. Dickey, M. J. McPhaden, R. R. Bidigare, M. R. Lewis, R. T. Barber, S. T. Lindley, C. Garside, D. V. Manov, and J. D. McNeil, Longwaves and primary production variations in the equatorial Pacific at 0°, 140°W, *Deep Sea Res., Part II, 44*, 1801–1826, 1997.

Francey, R. J., P. P. Tans, C. E. Allison, I. G. Enting, J. W. White, and M. Trolier, Changes in oceanic and terrestrial carbon uptake since 1982, *Nature, 373*, 326–330, 1995.

Fushimi, K., Variation of carbon dioxide partial pressure in the western North Pacific surface water during the 1982/83 El Niño event, *Tellus, Ser.B, 39*, 214–227, 1987.

Gaspar, P., Y. Gregoris, and J. M. Lefevre, A simple eddy kinetic energy model for simulations of the oceanic vertical mixing: Tests at station Papa and Long-Term Upper Ocean Study Site site, *J. Geophys. Res., 95*, 16,179–16,193, 1990.

Gibson, J. K., P. Källberg, S. Uppala, A. Hernandez, A. Nomura, and E. Serrano, ECMWF re-analysis project report series, 1, ERA description, *Project Rep. Series, 1*, 72 pp., Eur. Cent. for Medium-Range Weather forecast, Reading, England, 1997.

Goyet, C., and E. T. Peltzer, Comparison of the August-September 1991 and 1979 surface partial pressure of CO_2 distribution in the Equatorial Pacific Ocean near 150°W, *Mar., Chem., 45*, 257–266, 1994.

Goyet, C., and E. T. Peltzer, Variation of CO_2 partial pressure in surface seawater in the equatorial Pacific Ocean, *Deep Sea Res., Part I, 44*, 1611–1625, 1997.

Guilyardi, E., and G. Madec, Performance of OPA-ARPEGE-T21 global ocean-atmosphere coupled model, *Clim. Dyn., 13*, 149–165, 1997.

Hayes, S. P., L. J. Mangum, J. Picaut, A. Sumi, and K. Takeuchi, TOGA-TAO: A moored array for real-time measurements in the tropical Pacific Ocean, *Bull. Am. Meteorol. Soc., 72*, 339–347, 1991.

Hellermann, S., and M. Rosenstein, Normal monthly wind-stress over the world ocean with error estimates, *J. Phys. Oceanogr., 24*, 619–637, 1983.

Hurrell, J. W., Decadal trends in the North Atlantic Oscillation: Regional temperatures and precipitation, *Science, 269*, 676–679, 1995.

Inoue, H. Y., and Y. Sugimura, Variations and distributions of CO_2 in and over the equatorial Pacific during the period from the 1986/88 El Ninño event to the 1988/89 La Niña event, *Tellus, Ser.B, 44*, 1–22, 1992.

Inoue, H. Y., M. Ishii, H. Matsueda, M. Ahoyama, and I. Asanuma, Changes in longitudinal distribution of the partial pressure of CO_2 (pCO_2) in the central and western equatorial Pacific, west of 160°W, *Geophys. Res. Lett., 23*, 1781–1784, 1996.

Ishii, M., and H. Y. Inoue, Air-sea exchange of CO_2 in the central and western equatorial Pacific in 1990, *Tellus, Ser.B, 47*, 447–460, 1995.

Jacobs, G. A., and J. L. Mitchell, Ocean circulation variations associated with the Antarctic Circumpolar Wave, *Geophys. Res. Lett., 23*, 2947–2950, 1996.

Jianrong, Z., and P. D. Quay, The total organic carbon export rate based on ^{13}C and ^{12}C of DIC budgets in the equatorial Pacific region, *Deep Sea Res., Part II, 44*, 2163–2190, 1997.

Joos, F., M. Bruno, R. Fink, T. F. Stocker, U. Siegenthaler, C. Le Quéré, and J. L. Sarmiento, An efficient and accurate representation of complex oceanic and biospheric models of anthropogenic carbon uptake, *Tellus, Ser.B, 48*, 397–417, 1996.

Joos, F., R. Meyer, M. Bruno, and M. Leuenberger, The variability in the carbon sinks as reconstructed for the last 1000 years, *Geophys. Res. Lett., 26*, 1437–1440, 1999.

Kalnay, E., et al., The NCEP/NCAR 40-year reanalysis project, *Bull. Am. Meteorol. Soc, 77*, 437–471, 1996.

Karl, D. M., and R. Lukas, The Hawaii Ocean Time-series (HOT) program: Background, rationale and field implementation, *Deep Sea Res., Part II, 43*, 129–156, 1996.

Keeling, C. D., and R. Revelle, Effects of El Niño/Southern Oscillation on the atmospheric content of carbon dioxide, *Meteoritics, 20*, 437–451, 1985.

Keeling, C. D., R. B. Bacastow, A. F. Carter, S. C. Piper, T. P. Whorf, M. Heimann, W. G. Mook, and H. Roeloffzen, A three-dimensional model of atmospheric CO_2 transport based on observed winds; 1, Analysis of observational data, in *Aspects of Climate Variability in the Pacific and the Western Americas, Geophys. Monogr. Ser.*,

vol. 55, edited by D. H. Peterson, pp. 165–237, AGU, Washington, D. C., 1989.

Keeling, C. D., T. P. Whorf, M. Wahlen, and J. van der Plicht, Interannual extremes in the rate of rise of atmospheric carbone dioxide since 1980, *Nature, 375*, 666–670, 1995.

Ledwell, J. R., A. J. Watson, and C. S. Law, Mixing of a tracer in the pycnocline, *J. Geophys. Res., 103*, 21,499–21,530, 1998.

Lee, K., R. Wanninkhof, T. Takahashi, S. C. Doney, and R. A. Feely, Low interannual variability in recent oceanic uptake of atmospheric carbon dioxide, *Nature, 396*, 155–158, 1998.

Lefèvre, N., and Y. Dandonneau, Air-sea CO_2 fluxes in the equatorial Pacific Ocean in January-March 1991, *Geophys. Res. Lett., 19*, 2223–2226, 1992.

Le Quéré, C., Variabilité du carbone océanique de 1979 à 1997 : Modélisation et évaluation, Ph.D. thesis, Univ. Pierre et Marie Curie, Paris, 1999.

Levitus, S., Climatological atlas of the world ocean, *Tech. Rep. 13*, U.S. Govt. Print. Office, Washington D. C., 1982.

Liss, P. S., and L. Merlivat, Air-sea gas exchange: Introduction and synthesis, in *The Role of Air-Sea Exchange in Geochemical Cycling*, edited by P. Buat-Ménard, pp. 113-127, D. Reidel, Norwell, Mass., 1986.

Lohrenz, S. E., G. A. Knauer, V. L. Asper, M. Tuel, A. F. Michaels, and A. H. Knap, Seasonal variability in primary production and particle flux in the Northwestern Sargasso Sea: U.S. JGOFS Bermuda Atlantic Time-series Study, *Deep Sea Res., Part I, 39*, 1373–1391, 1992.

Louanchi, F., M. Hoppema, D. C. E. Bakker, A. Poisson, M. H. C. Stoll, H. J. W. de Baar, B. Schauer, D. P. Ruiz-Pino, and D. Wolf-Gladrow, Modelled and observed sea surface fCO_2 in the southern ocean: A comparative study, *Tellus, Ser.B, 51*, 541–559, 1999.

Madec, G., and M. Imbard, A global ocean mesh to overcome the North Pole singularity, *Clim. Dyn., 12*, 381–388, 1996.

Madec, G., P. Delecluse, M. Imbard, and C. Lévy, *OPA Version 8.0 Ocean General Circulation model*, reference manual, Lab. Océanogr. Dyn. and Climatol., Paris, 1997.

Maier-Reimer, E., Geochemical cycles in an ocean general circulation model: Preindustrial tracer distributions, *Global Biogeochem. Cycles, 7*, 645–677, 1993.

Maier-Reimer, E., U. Mikolajewicz, and A. Winguth, Future ocean uptake of CO_2: Interaction between ocean circulation and biology, *Clim. Dyn., 12*, 711–721, 1996.

Matear, R. J., and A. C. Hirst, Climate change feedback on the future oceanic CO_2 uptake, *Tellus, Ser.B, 51*, 722–733, 1999.

Mehrbach, C., C. H. Culberson, J. E. Hawley, and R. M. Pytkowicz, Measurement of the apparent dissociation constants of carbonic acid in seawater at atmospheric pressure, *Limnol. Oceanogr., 18*, 897–907, 1973.

Murnane, R. J., J. L. Sarmiento, and C. Le Quéré, Spatial distribution of air-sea CO_2 fluxes and the interhemispheric transport of carbon by the oceans, *Global Biogeochem. Cycles, 13*, 287–305, 1999.

Murphy, P. P., K. C. Kelly, R. A. Feely, and R. H. Gammon, Carbon dioxide concentrations in surface water and the atmosphere: PMEL cruises 1986-1989, *Tech. Rep. 1504*, Pac. Mar. Environ. Lab., NOAA, Seattle, Wash., 1994.

Murtugudde, R., S. R. Signorini, J. R. Christian, A. J. Busalacch, and C. R. McClain, Ocean color variability of the tropical Indo-Pacific basin observed by SeaWiFS, *J. Geophys. Res., 104*, 18,351–18,366, 1999.

Oberhüber, J. M., An atlas on the 'COADS' data set: The budget of heat, buoyancy, and turbulent kinetic energy at the surface of the global ocean, *Tech. Rep. 15*, Max-Planck Institut für Meteorologie, Hamburg, Germany, 1988.

Rayner, P., I. Enting, R. Francey, and R. Langenfelds, Reconstructing the recent carbon cycle from atmospheric CO_2, $\delta^{13}C$ and O_2/N_2 observations, *Tellus, Ser. B, 51*, 213–232, 1999.

Reynolds, R. W., and T. M. Smith, Improved global sea surface temperature analyses using optimum interpolation, *J. Clim., 7*, 929–948, 1994.

Roemmich, D., M. Morris, W. R. Young, and J. R. Donguy, Fresh equatorial jets, *J. Phys. Oceanogr., 24*, 540–558, 1994.

Sarmiento, J. L., Atmospheric co_2 stalled, *Nature, 365*, 697–698, 1993.

Sarmiento, J. L., and C. Le Quéré, Oceanic carbon dioxide uptake in a model of century-scale global warming, *Science, 274*, 1346–1350, 1996.

Sarmiento, J. L., J. C. Orr, and U. Siegenthaler, A perturbation simulation of CO_2 uptake in an ocean general circulation model, *J. Geophys. Res., 97*, 3621–3645, 1992.

Sarmiento, J. L., R. Murnane, and C. Le Quéré, Air-sea co_2 transfer and the carbon budget of the north Atlantic, *Philos. Trans. R. Soc. London, Ser. B, 348*, 211–219, 1995.

Sarmiento, J. L., T. M. C. Hughes, R. J. Stouffer, and S. Manabe, Simulated response of the ocean carbon cycle to anthropogenic climate warming, *Nature, 393*, 245–249, 1998.

Siegenthaler, U., and F. Joos, Use of a simple model for studying oceanic tracer distributions and the global carbon cycle, *Tellus, Ser.B, 44*, 186–207, 1992.

Six, K. D., and E. Maier-Reimer, Effects of plankton dynamics on seasonal carbon fluxes in an ocean general circulation model, *Global Biogeochem. Cycles, 10*, 559–583, 1996.

Smethie, W. M., T. Takahashi, D. W. Chipman, and J. R. Ledwell, Gas exchange and CO_2 flux in the tropical Atlantic ocean determined from 222 rn and pCO_2 measurements, *J. Geophys. Res., 90*, 7005–7022, 1985.

Smolarkiewicz, K. P., and T. L. Clark, The multidimensional positive definite advection transport algorithm: Further development and applications, *J. Comput. Phys., 67*, 396–438, 1986.

Stoens, A., C. Menkès, Y. Dandonneau, and L. Mémery, New production in the equatorial Pacific: a coupled dynamical-biogeochemical model, *Fish. Oceanogr., 7*, 311–316, 1998.

Suess, E., Particulate organic carbon flux in the ocean-surface productivity and oxygen utilization, *Nature, 288*, 260–263, 1980.

Takahashi, T., W. S. Broecker, and A. E. Bainbridge, The alkalinity and total carbon dioxide concentration in the World Oceans, in *Carbon Cycle Modeling in Scope*, edited by B. Bolin, pp. 271–286, John Wiley, New York, 1981.

Takahashi, T., J. Goddard, S. Southerland, D. W. Chipman, and C. C. Breeze, Seasonal and geographic variability of carbon dioxide sink/source in the ocean areas, Contract 19x.89675c, Lamont Doherty Geol. Obs., Palisades, New York, 1986.

Tans, P. P., et al., Climate Monitoring and Diagnostics Laboratory: Summary report 1994-95, *Tech. Rep. 23*, U.S. Dep. of Commer., Nat. Oceanic and Atmos. Admin. Environ. Res. Lab., Boulder, Colo., 1996.

Thoning, K. W., P. P. Tans, and W. D. Komhyr, Atmospheric carbon dioxide at Mauna Loa Observatory 2. Analysis of the NOAA GMCC data, 1974-1985, *J. Geophys. Res., 94*, 8549–8565, 1989.

Uppala, S., ECMWF Re-analysis Project Report Series 3 Observing system performance in ERA, *Project Rep. Series, 3*, Eur. Cent. for Medium-Range Weather forecast, Reading, England, 1997.

Verschell, M. A., Mechanisms of interannual CO_2 flux variability in the equatorial Pacific Ocean, *Tech. Rep. 96*, Cent. for Ocean-Atmos. Prediction Stud., Florida State Univ., Tallahassee, 1996.

Vialard, J., and P. Delecluse, An OGCM study for the TOGA decade, II: Barrier layer formation and variability, *J. Phys. Oceanogr.*, *28*, 1089–1106, 1998.

Volk, T., Effect of the equatorial Pacific upwelling on atmospheric CO_2 during the 1982-1983 El Ni no, *Global Biogeochem. Cycles*, *3*, 267–279, 1989.

Wanninkhof, R., Relationship between wind speed and gas exchange over the ocean, *J. Geophys. Res.*, *97*, 7373–7382, 1992.

Wanninkhof, R., R. A. Feely, H. Chen, C. Cosca, and P. P. Murphy, Surface water fCO_2 in the eastern equatorial Pacific during the 1992-1993 El Ni no, *J. Geophys. Res.*, *101*, 16,333–16,343, 1996.

Wanninkhof, R., E. Lewis, R. A. Feely, and F. J. Millero, The optimal carbonate dissociation constants for determining surface water pCO_2 (SST) from alkalinity and total inorganic carbon, *Mar. Chem.*, *65*, 291–301, 1999.

Weiss, R. F., Carbon dioxide in water and seawater: The solubility of a non-ideal gas, *Mar. Chem.*, *2*, 203–215, 1974.

Weiss, R. F., F. A. V. Woy, and P. K. Salame, Surface-water and atmospheric carbon dioxide and nitrous oxide observations by shipboard automated gas chromatography: Results from expeditions between 1977 and 1990, *Tech. Rep. NDP-044*, Carbon Dioxide Inf. Anal. Cent., Oak Ridge, Tenn., 1992.

White, W. B. and R. G. Peterson, An Antarctic circumpolar wave in surface pressure, wind, temperature and sea-ice extent, *Nature*, *380*, 699–702, 1996.

Winguth, A. M. E., M. Heimann, K. D. Kurz, E. Maier-Reimer, U. Mikolajewicz, and J. Segschneider, El Ni no-Southern Oscillation related fluctuations of marine carbon cycle, *Global Biogeochem. Cycles*, *8*, 39–63, 1994.

Wong, C. S., Y. H. Chang, J. S. Page, G. E. Smith, and R. D. Bellegay, Changes in equatorial CO_2 fluxes and new production estimated from CO_2 and nutrient levels in Pacific surface waters during the 1986/87 El Niño, *Tellus, Ser.B*, *45*, 64–79, 1993.

Yamanaka, Y., and E. Tajika, The role of the vertical fluxes of particulate organic matter and calcite in the oceanic carbon cycle: Studies using an ocean biogeochemical general circulation model, *Global Biogeochem. Cycles*, *10*, 361–382, 1996.

O. Aumont, P. Monfray, and J. C. Orr, Laboratoire des Sciences du Climat et de l'Environnement, Unité Mixte CEA-CNRS, CEA Saclay, L'Orme des Merisiers, Bat. 709, 91191 Gif-sur-Yvette, France.

C. Le Quére, Max Planck Institut fuer Biogeochemie, Carl Zeiss Promenade 10, 07745 Jena, Germany. (lequere@bgc-jena.mpg.de)

G. Madec, Laboratoire d'Océanologie Dynamique et de Climatologie, CNRS/ORSTOM/UPCM, Université Paris VI, 4 place Jussieu, Paris 75252 CEDEX 05, France.

(Received January 26, 1999; revised June 30, 1999; accepted July 21, 1999.)